Ciliary and extraciliary Gpr161 pools repress hedgehog signaling in a tissue-specific manner

Sun-Hee Hwang[1], Bandarigoda N. Somatilaka[1,2], Kevin White[1], and Saikat Mukhopadhyay[1*].

[1]Department of Cell Biology, University of Texas Southwestern Medical Center, Dallas, Texas, 75390.

[2]Present address: Department of Dermatology, University of Texas Southwestern Medical Center, Dallas, Texas, 75390.

[*]Correspondence:

Email: Saikat.Mukhopadhyay@utsouthwestern.edu

Running title: Tissue-specific functions of ciliary cAMP.

Impact statement:

Signaling by Cilia

Signaling by cAMP specifically in cilia directs tissue-specific morphogenesis

Abstract

The role of compartmentalized cAMP signaling in primary cilia is not well understood. The cilia-localized G-protein-coupled receptor—Gpr161 represses hedgehog pathway via cAMP signaling. Here, by generating knock-in mutant mouse at endogenous *Gpr161* locus (*mut1*), we show that ciliary and extraciliary receptor pools repress hedgehog signaling in a tissue-specific manner. Gpr161^{mut1} was competent in generating cAMP but did not transit through cilia. Compared to knockout, *Gpr161^{mut1}* had delayed embryonic lethality, less upregulation of hedgehog targets and partially down-regulated Gli3-repressor. Ventral-most progenitor expansion in neural tube of *Gpr161* knockout occurred in a Gli2-activator-dependent manner but was not seen in *Gpr161^{mut1}*. Intermediate-level ventralization occurred from Gpr161 lack specifically in cilia but was restored by increased extraciliary mutant generating Gli3-repressor. Morphogenesis in limb buds and midface that require Gli-repressor manifested hedgehog hyperactivation phenotypes—polydactyly and midfacial widening—in *Gpr161^{mut1}*. Thus, ciliary and extraciliary cAMP signaling establishes tissue-specific Gli-repressor thresholds in dictating morpho-phenotypic outcomes.

Keywords: Cilia; hedgehog; cAMP; Gpr161; Gli repressor; neural tube; craniofacial; limb bud; polydactyly, morphogenesis.

Introduction

The primary cilium is a paradigmatic organelle for studying compartmentalized cellular signaling in morphogenesis and disease (Anvarian et al., 2019; Nachury & Mick, 2019). The primary cilium is a microtubule-based dynamic cellular appendage that is templated from the mother centriole of the centrosome–the basal body, and is present in multiple cell types (Wang & Dynlacht, 2018). Cilia can transduce cellular response to extracellular signals, such as hedgehog (Hh) ligands (Huangfu et al., 2003), during differentiation and proliferation, regulating morphogenesis (Kopinke et al., 2020). Long considered vestigial, dysfunction of the primary cilium has now been implicated in diseases affecting diverse tissues, collectively termed “ciliopathies” (Reiter & Leroux, 2017). The tissue abnormalities include neural tube defects (Murdoch & Copp, 2010), limb/skeletal malformations (Huber & Cormier-Daire, 2012), craniofacial dysmorphisms (Brugmann, Cordero, et al., 2010), and heart defects (Gabriel et al., 2020), emphasizing ciliary role in diverse contexts.

The mechanisms by which cilia-specific signals are maintained and propagated to direct downstream pathways during morphogenesis is not well understood. Particularly, non-ciliary signaling by cilia localized proteins can be a confounding factor in understanding how signaling at and by cilia contributes to tissue phenotypes. Studying signaling at cilia requires mechanistic understanding of trafficking to cilia, isolating ciliary from extraciliary functions of signaling molecules, and studying functional consequences directly in tissues without disrupting cilia (Mukhopadhyay et al., 2017). Decoding the features of signaling unique to the primary cilium in directing downstream cellular pathways is necessary for understanding the pathogenesis of diseases caused by ciliary dysfunction.

The primary cilium mediates cellular signaling responses to Hh morphogens in vertebrates (Briscoe & Therond, 2013; Goetz & Anderson, 2010). An intricate balance between formation of Gli transcriptional activators and repressors determines the transcriptional output to Hh morphogens (Hui & Angers, 2011). Both responses are dependent on the primary cilium. Binding

of Hh to its receptor Patched (Ptch1) triggers removal of Ptch1 from cilia and promotes enrichment and activation of Smoothened (Smo)—the pathway transducer—in cilia, resulting in generation of Gli transcriptional activator (GliA) (Corbit et al., 2005; Rohatgi et al., 2007). In contrast, repression in the absence of Hh involves protein kinase A (PKA) initiated phosphorylation followed by limited proteolysis of full length Gli2/3 into Gli2/3 repressor (GliR) forms, also in a cilia-dependent manner (Mukhopadhyay & Rohatgi, 2014; Tuson et al., 2011). GliA/R regulation is also different in tissues and can be categorized as primarily occurring by GliA or GliR thresholds (Kopinke et al., 2020).

We previously described that the cilia-localized orphan G-protein-coupled receptor (GPCR), Gpr161 functions as a negative regulator of Hh signaling during early neural tube development in mice (Mukhopadhyay et al., 2013). Mice knockout for *Gpr161* are embryonic lethal by embryonic day 10.5 (E10.5) and exhibit increased Hh signaling and expansion of ventral progenitors throughout the rostrocaudal extent of the neural tube, without disrupting cilia. Gpr161 determines Gli3R formation via cAMP signaling. However, ventral part of the neural tube is mainly regulated by Gli2 and Gli3 activators (Bai & Joyner, 2001; Bai et al., 2004), only intermediate levels of neural tube are regulated by Gli3 repressor (Persson et al., 2002). We recently also described roles of Gpr161 in forelimb formation, skeletal development (Hwang et al., 2018), embryonic cerebellar development (Shimada et al., 2018), and forebrain development (Shimada et al., 2019). Tissues such as the limbbuds and cerebellum show GliR gradients preceding sonic hedgehog (Shh) expression (Kopinke et al., 2020), where *Gpr161* deletion resulted in lack of GliR (Hwang et al., 2018; Shimada et al., 2018). Thus, *Gpr161* deletion can induce high Hh signaling phenotypes in tissues that are regulated by loss of GliR and/or from GliA formation.

Gpr161 localizes to the ciliary membrane dynamically and also to the recycling endocytic compartment (Mukhopadhyay et al., 2013; Pal et al., 2016). However, whether Gpr161 functions from inside the primary cilium and/or in the endomembrane compartment in regulating cAMP-PKA signaling and Hh pathway phenotypes during morphogenesis is not clear. Importantly, the phenotypes in all affected tissues from *Gpr161* deletion were rescued from concomitant loss of

cilia (Hwang et al., 2018; Mukhopadhyay et al., 2013; Shimada et al., 2018) indicating that the effects of the lack of cAMP signaling were strictly cilia dependent. Interestingly, Gpr161 C-tail has been proposed to be an A-kinase anchoring protein (AKAP) for PKA activation in cilia by binding to type I PKA regulatory subunits (Bachmann et al., 2016). The PKA regulatory subunit RIα and RII localizes to cilia (Bachmann et al., 2016; Mick et al., 2015) and centrosomes (Barzi et al., 2010; Saade et al., 2017; Tuson et al., 2011), respectively, whereas PKA-c localizes to centrosomes (Barzi et al., 2010; Saade et al., 2017; Tuson et al., 2011) and cilia (Truong et al., 2021). Gpr161 is the only GPCR known to be an AKAP. Precise regulation of Gpr161 pools inside and/or outside cilia is required to address role of subcellular compartmentalization of cAMP in morpho-phenotypic outcomes.

Here, we generated ciliary localization defective but signaling competent *Gpr161*^{mut1} knock-in mice. We demonstrated the tubby family protein Tulp3 (Badgandi et al., 2017; Mukhopadhyay et al., 2010) as a key adapter that traffics multiple types of cargoes into ciliary membrane without affecting total cargo pools. The *Gpr161* knock-in mutant was based on the Tulp3-targeted ciliary localization sequence that we had previously identified (Mukhopadhyay et al., 2013). Using this knock-in model, we demonstrate that tissues that require GliR for morphogenesis, such as mid face and limb buds, are affected from loss of Gpr161 ciliary pools showing mid face widening and polydactyly. In the neural tube, intermediate level patterning that is regulated by Gli3R is affected in *Gpr161*$^{mut1/ko}$ embryos, but ventral-most patterning that is GliA regulated remains unaffected. Our findings indicate that ciliary Gpr161 pools prevent Hh pathway hyperactivation phenotypes specifically from GliR lack but not from GliA generation.

Results

A ciliary localization-defective *Gpr161* mutant is signaling-competent

We previously described the (V/I)KARK motif in the third intracellular loop of Gpr161 to be necessary and sufficient for targeting to cilia by the tubby family protein Tulp3 (**Figure 1A**) (Badgandi et al., 2017; Mukhopadhyay et al., 2010; Mukhopadhyay et al., 2013). We used NIH 3T3 cells that are knockout for *Gpr161* (Pusapati et al., 2018) to stably overexpress untagged wildtype *Gpr161* and *Gpr161*^{mut1} (VKARK>AAAAA; Gpr161^{mut1}). Wildtype Gpr161 predominantly localized to cilia. In contrast, Gpr161^{mut1} was not localized to cilia but was observed in vesicles, some of which surrounded the base of cilia (**Figure 1B**).

We previously demonstrated that Tulp3 regulates trafficking of Gpr161 into cilia but does not affect trafficking out of cilia (Badgandi et al., 2017). We conclusively ruled out that LAP-tagged Gpr161^{mut1} (LAP, S tag-PreScission-GFP) does not at all transit through cilia by immunostaining for GFP using the following three approaches to promote accumulation of ciliary pools and/or prevent trafficking out of cilia.

First, loss of the 5'phosphatase, Inpp5e, increases levels of Tulp3, IFT-A complex subunits and Gpr161 in the ciliary membrane (Chavez et al., 2015; Garcia-Gonzalo et al., 2011) likely from defects in Tulp3 cargo release (Badgandi et al., 2017). If Gpr161^{mut1} transits through cilia but is too low to detect at steady state, we would expect to see it accumulating upon Inpp5e loss. By stably expressing the mutant LAP-tagged wild type (*Gpr161*^{wt}) and *Gpr161*^{mut1} in RPE hTERT cells, we confirmed the *Gpr161*^{mut1} fusion to be not localizing to cilia unlike *Gpr161*^{wt} (**Figure 1C-D**). As expected, upon *INPP5E* knockdown, we saw accumulation of endogenous TULP3 and LAP-tagged Gpr161^{wt} in cilia (**Figure 1C-F**). However, we did not see any accumulation of LAP-tagged *Gpr161*^{Mut1} in cilia (**Figure 1C-E**), despite accumulation of TULP3 (**Figure 1F**).

Second, Gpr161 is accumulated in β–arrestin 1/2 double knockout (*Arrb1/Arrb2* dko*)* MEFs as β–arrestins regulate Gpr161 removal from cilia (Pal et al., 2016). If Gpr161^{mut1} transits

through cilia, lack of β–arrestins should prevent removal from cilia promoting ciliary accumulation. We stably expressed LAP-tagged *Gpr161*^{wt} and *Gpr161*^{mut1} in wild type and *Arrb1/Arrb2* dko MEFs (Kovacs et al., 2008) (**Figure 1-figure supplement 1**). LAP-tagged Gpr161^{wt} localized to cilia and was removed upon treatment with Smoothened agonist SAG but was accumulated in dko cells, as reported earlier (Pal et al., 2016). However, LAP-tagged Gpr161^{mut1} did not accumulate in cilia of wild type or dko MEFs. Accumulation of endogenous Gpr161 in the *Arrb1/Arrb2* dko MEFs expressing LAP-tagged Gpr161^{mut1}, surmised from Gpr161 immunostaining in absence of any GFP in cilia, was still observed.

Third, the BBS-ome has been shown to regulate exit of Gpr161 from cilia (Ye et al., 2018) and knockdown of BBS-ome subunits result in accumulation of Gpr161 in cilia (Nozaki et al., 2018). If Gpr161^{mut1} transits through cilia, lack of BBS subunits should prevent exit from cilia promoting ciliary accumulation. Stably expressed LAP-tagged Gpr161^{wt} localized to cilia and was accumulated upon BBS4 knockdown in RPE-hTERT cells. However, stably expressed LAP-tagged Gpr161^{mut1} did not accumulate in cilia even upon *BBS4* knockdown (**Figure 1-figure supplement 2**).

We had previously demonstrated wild type Gpr161 containing vesicles to be recycling endosomes that co-label with endocytosed fluorescent transferrin (Mukhopadhyay et al., 2013). We noted that LAP-tagged Gpr161^{mut1} containing vesicles co-labeled with endocytosed fluorescent transferrin, similar to LAP-tagged Gpr161^{wt} (**Figure 1-figure supplement 3**). Thus, the propensity of the receptor to reside in recycling endosomes is not affected even in the absence of transit of Gpr161^{mut1} through cilia.

Agonist-independent constitutive signaling has been observed for a wide variety of GPCRs (Leurs et al., 1998; Seifert & Wenzel-Seifert, 2002). In the absence of a known ligand, we previously demonstrated constitutive activity of the orphan Gpr161 by generating doxycycline-inducible stable cell lines expressing the untagged wild-type receptor (Mukhopadhyay et al., 2013). We used a similar strategy to generate a doxycycline-inducible line expressing untagged

Gpr161^{mut1}. We used a TR-FRET cAMP assay (Cisbio) for estimating cAMP levels. These assays eliminate the background noise due to FRET-based estimation of signals, and the use of long-lived fluorophores (in this case lathanides), combined with time-resolved FRET detection (a delay between excitation and emission detection) minimizes prompt intrinsic fluorescence interferences (Degorce et al., 2009). Gpr161^{mut1} demonstrated comparable constitutive cAMP signaling activity compared to the wild-type receptor (**Figure 1G**), suggesting that the ciliary localization defective GPCR was signaling competent. Thus, the *Gpr161*^{mut1} mutant allows to uncouple cAMP signaling function from ciliary localization of Gpr161.

Generating ciliary localization defective endogenous knock-in *Gpr161*^{mut1} mouse model

We next generated a mouse knock-in allele of *Gpr161*^{mut1} in the endogenous locus and confirmed the endogenous integration by southern blotting (**Figure 2A-B**) and sequencing (**Figure 2C**). We engineered a NotI restriction site in the mutated *Gpr161*^{mut1} exon 4 sequence (**Figure 2-figure supplement 1**) for genotyping using RFLP assays (**Figure 2A, 2D**). We bred the knock-in alleles with *Gpr161* knockout (ko) allele. Quantitative RT-PCR of *Gpr161* transcripts in E9.5 embryos suggested that the *Gpr16*^{mut1} transcript was expressed at similar levels compared to wild type and was reduced to 50% compared to wildtype in *Gpr161*$^{ko/mut1}$ embryos (**Figure 2E**). *Gpr161*$^{ko/ko}$ embryos lacked *Gpr161* transcripts, as expected.

We were unable to determine protein levels of the endogenous mutant receptor in the *Gpr161*^{mut1} embryos due to technical constraints in immunoblotting for endogenous levels**.** However, we note Gpr161^{mut1} in vesicles surrounding the base of cilia (**Figure 1B**) and constitutive cAMP signaling activity (**Figure 1G**) in stable cell lines, suggesting that protein levels and activity of the mutant were comparable with wild type Gpr161. We stably overexpressed LAP-tagged Gpr161^{wt} and Gpr161^{mut1} in wild type MEFs and performed tandem affinity purification followed by immunoblotting to detect the proteins. We noted similar immunoblotting pattern from receptor glycosylation in both variants (**Figure 2-figure supplement 2**).

We previously reported that the morphology of cilia was not grossly affected in the *Gpr161* *k*nockout or conditional knockout embryos (Hwang et al., 2018; Mukhopadhyay et al., 2013). The ciliary morphologies, including ciliary lengths in *Gpr161*$^{ko/mut1}$ embryos in mesenchyme, somatopleuric mesoderm or in the neural tube were similarly unaffected (**Figure 2-figure supplement 3**).

Gpr161^{mut1} allele is hypomorphic to knockout

Mice homozygous for *Gpr161* ko allele are embryonic lethal by E10.5 with extensive craniofacial abnormalities, open forebrain and midbrain regions, and lack of forelimbs (Hwang et al., 2018; Mukhopadhyay et al., 2013) (**Figure 3A**). In contrast, the *Gpr161*$^{mut1/ko}$ mice were embryonic lethal by E13.5 (**Table 1**). The *Gpr161*$^{mut1/ko}$ embryos had craniofacial abnormalities, microphthalmia (**Figure 3A-C**) and spina bifida similar to *Gpr161* ko (**Figure 3B**) along with kinked tail, often associated with caudal neural tube defects (**Figure 3C**). They also had stunted forelimbs (**Figure 3B-C**) and heart defects with pericardial effusion (**Figure 3C**). However, the *Gpr161*$^{mut1/mut1}$ mice were embryonic lethal by E14.75 (**Table 1**) with craniofacial abnormalities including mid face widening, microphthalmia (**Figure 3D-E**) and polydactyly in both forelimbs and hindlimbs (**Figure 3D**). Thus, the *Gpr161*^{mut1} allele is hypomorphic to *Gpr161* ko. The *Gpr161*$^{mut1/mut1}$, *Gpr161*$^{mut1/ko}$ and *Gpr161*$^{ko/ko}$ embryos give rise to an allelic series increasing in phenotypic severity (**Table 2**).

Gpr161$^{mut1/ko}$ embryos have reduced Hh pathway hyperactivation compared to knockouts

As *Gpr161*^{mut1} allele is later embryonic lethal compared to knockout, we tested if Hh signaling is impacted in *Gpr161* mutants by analyzing the expression of direct transcriptional targets of the Hh pathway, *Gli1* and *Patched2* (*Ptch2*). In whole embryo extracts at E9.5, we detected increased levels of both transcripts in the *Gpr161*$^{ko/ko}$ embryos, intermediate levels in *Gpr161*$^{mut1/ko}$ embryos, and slightly elevated levels but statistically insignificant from wild type in *Gpr161*$^{mut1/mut1}$ embryos (**Figure 4A-B**). Gli1 protein levels also showed similar trends (**Figure 4C**). These data indicate

that *Gpr161* knock-in mutants experience gradually decreasing levels of Hh pathway hyperactivity compared to ko, commensurate with monoallelic or biallelic expression of *Gpr161*^{mut1}.

Gpr161$^{mut1/ko}$ embryos have intermediate GliR levels compared to knockouts

In the absence of Hh ligand, PKA-mediated phosphorylation of Gli3 results in its limited proteolysis into Gli3R (Niewiadomski et al., 2014; Tempe et al., 2006; Wang et al., 2000). In *Gpr161*$^{ko/ko}$ embryos, the extent of Gli3 processing into Gli3R at E9.5 whole-embryonic extracts was strongly decreased compared to wild type, suggesting that Gpr161 directs processing of Gli3 into Gli3R (Hwang et al., 2018; Mukhopadhyay et al., 2013). Compared to wild-type, the extent of Gli3 processing into Gli3R at E9.5 whole-embryonic extracts was strongly decreased in *Gpr161*$^{ko/ko}$ and *Gpr161*$^{ko/mut1}$ embryos, and trended towards decreased levels, but were not statistically significant in the *Gpr161*$^{mut1/mut1}$ embryos. Upon Hh signaling limited proteolysis of Gli3 is prevented, whereas activated full-length Gli proteins are formed that are unstable (Chen et al., 2009; Humke et al., 2010; Jia et al., 2009; Wang et al., 2010; Wen et al., 2010). Compared to wild type, Gli3 full-length forms trended towards decrease in *Gpr161*$^{ko/mut1}$ and *Gpr161*$^{mut1/mut1}$ embryos but were not statistically significant (**Figure 4C**). Gli3 full-length to Gli3R ratios were significantly increased in both *Gpr161*$^{ko/ko}$ and *Gpr161*$^{ko/mut1}$ embryos with respect to wild type (**Figure 4C**). Gli2R levels were only moderately reduced in *Gpr161*$^{ko/ko}$ embryos at E9.5, while being less affected in the *Gpr161*$^{ko/mut1}$ and *Gpr161*$^{mut1/mut1}$ embryos (**Figure 4-figure supplement 1**). In summary, the *Gpr161* mutants exhibit gradually decreasing severity of Gli3 processing defects compared to ko, commensurate with monoallelic or biallelic expression of *Gpr161*^{mut1}.

Gpr161^{mut1} NIH 3T3 cells exhibit Gli2 accumulation in cilia similar to *Gpr161* knockouts

Upon Hh pathway activation, Gli2 proteins accumulate at the tips of cilia (Chen et al., 2009; Haycraft et al., 2005; Kim et al., 2009). While ~20% of cilia tips in control cells had detectable Gli2 staining, treatment with SAG increased Gli2 accumulation in control cilia in NIH 3T3 cells (**Figure 4D-E**). In contrast, ~60% of *Gpr161* ko cilia in NIH 3T3 cells had Gli2 staining irrespective of SAG

treatment (**Figure 4D-E**). Stable expression of wild type *Gpr161* (*Gpr161*^{wt}), but not that of *Gpr161*^{mut1}, rescued the basal Gli2 ciliary accumulation in *Gpr161* ko cells. Thus, basal Gli2 accumulation in ciliary tips occurs from the absence of ciliary Gpr161 pools.

Gpr161$^{mut1/ko}$ embryos exhibit less ventralized neural tube compared to _Gpr161_ knockouts

The neural tube is patterned during early embryonic development by Hh secreted from the notochord. The neuroprogenitors acquire different spatial identities along the dorso-ventral axis due to a complex interplay of transcription factors, which are expressed in response to relative variations in Hh levels, as well as the duration for which they are exposed (Dessaud et al., 2008). As we had demonstrated before (Mukhopadhyay et al., 2013), Hh-dependent ventral cell types were ectopically specified at the expense of lateral and dorsal cell types (ventralization) in the *Gpr161*$^{ko/ko}$ at E9.5 (**Figure 5**). Specifically, floor plate progenitors expressing FoxA2, and p3/pMN/p2 progenitors expressing Nkx6.1 showed enlarged expression domains, expanding into comparatively more dorsal regions throughout the rostrocaudal extent of the spinal cord and hindbrain (**Figure 5, Figure 5-figure supplement 1**). The dorsolateral neural tube marker Pax6 was expressed in dorsally restricted domains, whereas Pax7 was strongly downregulated (**Figure 5**).

Ventral-most neural tube patterning is dependent on the downstream activation of Gli2 (Bai & Joyner, 2001), whereas intermediate-level patterning is Gli3R regulated (Persson et al., 2002). We investigated if the *Gpr161* ko phenotype is dependent on Gli2 by generating *Gpr161; Gli2* double ko. We generated linked double mutants by recombination, as *Gpr161* and *Gli2* genes are on the same chromosome. *Gli2* single ko is perinatal lethal (Bai & Joyner, 2001). The *Gpr161; Gli2* double ko survived till E12.75, past the embryonic lethality period for *Gpr161* single ko at E10.5. The double ko embryos also exhibited exencephaly, similar to *Gpr161* ko (**Figure 5**), suggesting a possible role for Gli3 in this region (Liu et al., 2015; Shimada et al., 2019; Yu et al., 2009).*Gli2* ko shows sparse FoxA2 expression in the floorplate throughout the rostrocaudal extent

of the neural tube without affecting Nkx6.1, compared to wild type (Somatilaka et al., 2020). The double ko had reduced FoxA2 in floor plate compared to *Gpr161* ko, suggesting that ventralization requires Gli2A. However, persistent but limited ventralization of Nkx6.1 domain suggested independence from Gli2A (**Figure 5, Figure 5-figure supplement 1**). The dorsolateral markers Pax7 and Pax6 were both partially restored compared to *Gpr161* ko (**Figure 5**). Another negative regulator that we recently described, Ankmy2, an ankyrin repeat and MYND domain protein, functions by regulating adenylyl cyclase trafficking to cilia (Somatilaka et al., 2020). Ventral expansion of the floor plate progenitors in *Ankmy2* knockout, even though being more severe than *Gpr161* knockout, is fully Gli2-dependent. However, intermediate level expansion of Nkx6.1 persisted upon concomitant Gli2 loss in *Ankmy2* knockout, suggesting a role of lack of Gli3R. Thus, ventralization of FoxA2 in *Gpr161* ko is Gli2-dependent, whereas Nkx6.1 domain ventralization is likely to be Gli3R-dependent.

As we had detected a partial hyperactivation of Hh targets and decrease in Gli3R levels in $Gpr161^{ko/mut1}$ whole embryo lysates (**Figure 4**), we next compared the neural tube phenotypes of $Gpr161^{ko/mut1}$ and $Gpr161^{mut1/mut1}$ embryos with $Gpr161^{ko/ko}$ and *Gpr161; Gli2* double ko. In contrast to $Gpr161^{ko/ko}$, $Gpr161^{ko/mut1}$ embryos had normal FoxA2 expression limited to floor plate. However, Nkx6.1 was expanded dorsally, although lesser in extent than in $Gpr161^{ko/ko}$. Pax6 was not dorsally restricted, whereas Pax7 was restored, unlike $Gpr161^{ko/ko}$ (**Figure 5**). Neural tube patterning in $Gpr161^{mut1/mut1}$ embryos was almost similar to wild type, except for a more restricted mid-dorsal expression of Pax7 (**Figure 5**). Thus, ventral-most FoxA2 patterning was unaffected in $Gpr161^{ko/mut1}$ and $Gpr161^{mut1/mut1}$ embryos, unlike *Gpr161* ko, suggesting that ventral-most progenitor expansion that requires Gli2A does not occur upon loss of ciliary Gpr161 pools. The persistence of limited Nkx6.1 ventralization in $Gpr161^{ko/mut1}$ and *Gpr161; Gli2* double ko phenocopies lack of Gli3 repressor (Persson et al., 2002). The Nkx6.1 domains were unaffected in $Gpr161^{mut1/mut1}$ embryos (**Figure 5, Figure 5-figure supplement 1**) from likely restoration of Gli3R at this embryonic stage (**Figure 4C**). Thus, ciliary pools of Gpr161 are required for

generating sufficient Gli3R levels to prevent such intermediate level ventralization. Increased extraciliary Gpr161 pools in *Gpr161*$^{mut1/mut1}$ also prevent Nkx6.1 ventralization from likely restoration of Gli3R processing.

Gpr16$^{mut1/mut1}$ embryos exhibit high Hh signaling and polydactyly in limb buds

As neural tube patterning defects were minimal in *Gpr161*$^{mut1/mut1}$ embryos, we tested if other tissues affected by Hh signaling were affected. *Shh* is expressed from the zone of polarizing activity (ZPA) in posterior limb buds from E9.75 (Charite et al., 2000) and patterns the digits (Niswander, 2003). Mutual antagonism between Gli3R and the bHLH transcription factor, dHand prepatterns the mesenchyme before *Shh* expression in posterior expression of 5' *Hoxd* genes (te Welscher et al., 2002). dHand also drives Shh expression from ZPA (Charite et al., 2000).

Gpr161$^{ko/ko}$ embryos lack forelimbs and have increased Shh signaling in the hind limbs (Hwang et al., 2018). Depletion of *Gpr161* in the limb mesenchyme using *Prx1-Cre* (*Prx1-Cre; Gpr161*$^{f/f}$) results increased expression of *Ptch1/Gli1* in both anterior and posterior forelimb fields and ectopic expression of Shh anteriorly. In contrast to *Gpr161*$^{ko/ko}$, forelimb buds were formed in *Gpr161*$^{mut1/mut1}$ embryos, and as in *Prx-Cre; Gpr161*$^{f/f}$ there was increased expression of *Ptch1/Gli1* in both anterior and posterior forelimb and hindlimb fields, as detected by RNA in-situ hybridization (ISH) (**Figure 6A**). Several features suggested a lack of Gli3R antagonism in causing Shh pathway hyperactivation. First, Shh was diffusely expressed posteriorly at E10.5 as detected by RNA ISH (**Figure 6B**), a likely result of dHand misexpression from Gli3R lack. Ectopic anterior expression of Shh in *Prx1-Cre; Gpr161*$^{f/f}$ is also likely from Gli3R lack that manifests later in the limb mesenchyme (Hwang et al., 2018). Second, *Hoxd13* expression by RNA ISH was anteriorly expanded in *Gpr161*$^{mut1/mut}$ embryos at E10.5 (**Figure 6C**), a likely result of lack of Gli3R antagonism (te Welscher et al., 2002). Third, we noticed a reduction of Gli3R formation in limb buds of *Gpr161*$^{mut1/mut1}$ embryos by immunoblotting at E12.5 (**Figure 6D**).

By E13.5, *Prx1-Cre; Gpr161*$^{f/f}$ had increased number of digit fields resulting in

polysyndactylous phenotypes (Hwang et al., 2018) (**Figure 6E**). *Gpr161*$^{mut1/mut1}$ embryos also showed polydactyly in both forelimb and hindlimb buds as apparent from RNA ISH for *Sox9* and *Col2a1* for mesenchymal and chondrogenic condensations, respectively (**Figure 6E**). Thus, lack of Gli3R in *Gpr161*$^{mut1/mut1}$ embryos is sufficient to cause increased Shh signaling and polydactyly.

Gpr161$^{mut1/mut1}$ embryos show high Hh signaling and mid face widening

Similar to limb bud patterning we tested if other tissues affected by lack of Gli repressor are similarly affected from loss of ciliary pools of Gpr161. Loss of cilia in cranial neural crest cells causes midfacial widening, duplicated nasal septum and bilateral cleft secondary palate (Brugmann, Allen, et al., 2010; Chang et al., 2016). Deletion of both *Gli2* and *Gli3* phenocopies these phenotypes, which are restored by expression of Gli3R (Chang et al., 2016), suggesting that ciliary signaling regulate GliR formation that is important in morphogenesis of this tissue. While lack of cilia in *Wnt1-Cre; Kif3a*$^{f/f}$ mutants shows lack of Gli2/3R levels, expression of *Ptch1* and *Gli1* are asynchronized, and are not reflective of the lack of repression (Chang et al., 2016).

Cranial neural crest-specific deletion of *Gpr161* using *Wnt1-Cre* resulted in microphthalmia, severe midfacial cleft and widening (**Figure 7A, D**). Similar midfacial widening as evident from increased distance between nasal pits was also observed in the *Gpr161*$^{mut1/mut1}$ embryos (**Figure 7B-E**). The midfacial widening resulted from increased gap between maxillary processes by ingression of median nasal processes (**Figure 7B-C**). *Gpr161*$^{mut1/mut1}$ embryos had high Hh signaling in craniofacial structures including nasopharangeal processes, palatal shelves and tongue, as evident from high *Ptch1* transcript levels by RNA ISH (**Figure 7B**). We also noted increased *Gli1* levels in the tongue of *Gpr161*$^{mut1/mut1}$ embryos by RNA ISH (**Figure 7C**). *Gpr161; Gli2* double ko embryos also showed midfacial widening and high *Ptch1* transcript levels by RNA ISH in the nasopharangeal processes (**Figure 7F**). Thus, high Hh signaling and midfacial widening from loss of Gpr161 ciliary pools was not Gli2A-dependent but was likely from GliR lack.

Discussion

Gpr161^{mut1} establishes an allelic series in regulating Hh pathway derepression

Hh signaling is regulated by GliA and GliR levels. GliA/R are generated from the same parental template, which makes their formation inter-dependent. Thus, GliA formation is inherently dependent on suppressed GliR processing (Pan et al., 2006) and phenotypes from GliR processing defects, such as in *Gpr161/Ankmy2* ko or in *PKA* null embryos can result from GliR loss or GliA formation (Kopinke et al., 2020). We generated a Gpr161^{mut1} receptor variant that did not transit through cilia but demonstrated constitutive cAMP signaling activity like wild type. The gradually decreasing severity of Hh pathway transcriptional upregulation and Gli3R processing defects among *Gpr161* ko, *Gpr161$^{mut1/ko}$* and *Gpr161$^{mut1/mut1}$* embryos establishes an allelic series for *Gpr161*, showing that both ciliary and extraciliary receptor pools function as a rheostat in regulating Hh signaling strength. The distinct phenotypic consequences in different tissues, however, argues for threshold specific response to GliA/R levels. Ventral-most progenitor expansion in neural tube is seen in absence of Gpr161 and is Gli2-dependent. Lack of Gpr161 ciliary pools specifically was incapable of generating sufficient GliA required for ventral-most progenitor expansion (**Figure 8A**). Intermediate-level Nkx6.1 ventralization occurred from loss of ciliary Gpr161 (**Figure 8A**), but such expansion could be suppressed by increased extraciliary Gpr161^{mut1} that generated Gli3R. Tissue regions that depend predominantly on Gli repressor were also specifically affected from loss of ciliary pools of Gpr161. These regions included the developing limb buds and face (**Figure 8B-C**). Collectively, effects of ciliary loss of Gpr161 pools are tissue specific and dependent on the requirements of the tissues on GliR vs GliA in morphogenesis. Tissue-specific Gli3R thresholds established by ciliary and extraciliary Gpr161 dictate morpho-phenotypic outcomes.

A recent study (Truong et al., 2021) used elegant optogenetic approaches regulating subcellular cAMP and genetic approaches subcellularly expressing dominant negative PKA to

study Shh-mediated somite patterning in zebrafish (Wolff et al., 2003). They showed that ciliary, but not cytoplasmic, production of cAMP functions through PKA localized in cilia to repress Shh-mediated somite patterning. Here we show that lack of ciliary Gpr161 pools, likely through cAMP signaling, result in Hh hyperactivation phenotypes from GliR loss in specific tissues or regions. However, we also find that the ventral neural tube is unaffected in patterning from lack of ciliary Gpr161 pools, presumably from deficient Gli2A formation that requires complete Gpr161 loss. Overall, our results are strikingly complementary to the optogenetic study by showing that lack of ciliary Gpr161 pools result in Hh hyperactivation phenotypes arising mainly from lack of GliR in the limb buds, mid-face and intermediate neural tube.

Currently, a limitation of the *Gpr161*^{mut1} allele arises from the fact that a physiological ligand, if any, for Gpr161 is unknown. Thus, we are unable to test role of Gpr161^{mut1} in ligand-induced signaling and formally rule out if this mutant is functioning as a hypomorph, in addition to being extraciliary. Another limitation of any approach that perturbs subcellular pools of cAMP, be it through genetic, optogenetic or chemogenetic means (Guo et al., 2019; Hansen et al., 2020; Truong et al., 2021), arises from the cilioplasm not being isolated from the cytoplasm. The second messengers, cAMP and Ca^{2+}, are both freely diffusible between ciliary and extraciliary compartments (Delling et al., 2016; Truong et al., 2021). Therefore, in any of these approaches, extraciliary cAMP could diffuse into ciliary compartments and vice versa. The contribution of the leaked cAMP from extraciliary cAMP production in *Gpr161*$^{mut1/mut}$ in the consequent phenotypes is unknown. However, the concentrations achieved from such leaks might not reach critical thresholds required for downstream PKA signaling at cilia (Truong et al., 2021).

Subcellular expression of Gpr161 variants is also likely to lead to increased specificity of localized cAMP action compared to optogenetic approaches increasing diffusible cAMP. The textbook model of cAMP causing dissociation of PKA catalytic subunits from regulatory subunits (Walsh & Cooper, 1979) is unlikely to occur in subcellular contexts based on the following

evidence. First, at physiological concentrations of cAMP (1-2 μm), most PKA catalytic subunits remain associated with regulatory subunits (Smith et al., 2017). Full dissociation occurs only at supraphysiological concentration. Second, physiological agonists causing native production of cAMP does not promote catalytic subunit release (Smith et al., 2017). Third, PKA signaling is sustained when catalytic and regulatory subunits are constrained (Smith et al., 2017). Fourth, released catalytic subunits are also rapidly recaptured by regulatory subunits after activation (Mo et al., 2017; Walker-Gray et al., 2017). Instead, the PKA regulatory subunit-AKAP complexes are fundamentally important in organizing and sustaining PKA catalytic subunit activation for localized substrate phosphorylation in restrictive nanodomains (Bock et al., 2020; Zhang et al., 2020). There have been conflicting reports of ciliary cAMP concentration ranging from levels comparable to that in the cytoplasm (Jiang et al., 2019) to supraphysiological levels ~4.5 μM (Moore et al., 2016) in kidney epithelial cells. Nonetheless, the dual functions of Gpr161 in Gαs coupling and as an atypical AKAP would further restrict PKA signaling in microdomains.

Gpr161 ciliary and extraciliary pools cumulatively contribute to Gli-repressor formation

Gpr161 pools both inside and outside cilia cumulatively contribute to Gli3R processing, with increased outside pools in *Gpr161*$^{mut1/mut1}$ embryos increasing processing levels compared to *Gpr161*$^{mut1/ko}$ embryos at E9.5 (**Figure 8D**). However, Gli3R processing defects in embryo and tissue settings for *Gpr161* and *Ankmy2* deletions in mouse and/or zebrafish (Hwang et al., 2018; Mukhopadhyay et al., 2013; Shimada et al., 2018; Shimada et al., 2019; Somatilaka et al., 2020; Tschaikner et al., 2019; Tschaikner et al., 2021) cannot be reliably modeled in *Gpr161* ko and *Ankmy2* ko NIH 3T3 or 3T3-L1 cells (Pusapati et al., 2018; Somatilaka et al., 2020). Despite contribution from both ciliary and extraciliary pools of Gpr161 in Gli3R processing, neural tube ventralization in *Gpr161* ko is completely dependent on cilia. Therefore, Gpr161 activity outside cilia in the *in vivo* settings is probably through the periciliary recycling endosomal compartment where it localizes in addition to cilia (Mukhopadhyay et al., 2013) and could activate ACs and PKA

in proximity to the centrosome (**Figure 8D**). Production of cAMP by Gpr161 in the endomembrane compartment, as reported for other GPCRs (Calebiro et al., 2009; Crilly & Puthenveedu, 2020; Irannejad et al., 2013; Kotowski et al., 2011; Vilardaga et al., 2014), could be relevant in cumulatively contributing to Gli3R processing. Direct Gpr161 C-tail binding to type I PKA regulatory subunits (Bachmann et al., 2016) is likely to facilitates PKA activation in proximity to Gpr161-mediated cAMP production in cilia for GliR processing (May et al., 2021; Mick et al., 2015), but if such coupling happens in the endomembrane compartment is not known.

Gpr161$^{mut1/mut1}$ limb buds showed decreased Gli3R processing compared to whole embryo lysates, suggesting limited compensation by extracellular Gpr161 pools in the limb buds and tissue specificity in contribution of extracellular Gpr161 pools to Gli3R processing. Phosphorylation by PKA in six Gli2/3 C-terminal clusters further primes phosphorylation by glycogen synthase kinase 3β and Casein kinase 1 (Tempe et al., 2006). Currently, subcellular location for these sequential phosphorylation events in Gli3R processing is not known (Kopinke et al., 2020). Precise cataloging of the phosphorylation cluster modifications in individual tissues would be required to determine tissue specificity in Gli3R processing efficiency.

Gpr161 subcellular pools uncouple Gli2 accumulation in cilia from activator formation

C-term phosphorylation of Gli2/3 proteins causes GliR formation, whereas GliA formation is dependent on lack of C-term phosphorylation by PKA (Niewiadomski et al., 2014). Expressing a *Gli2* mutant that is PKA-nonphosphorylatable has been shown to induce chick neural tube ventralization (Niewiadomski et al., 2014). Gli2A formation is compromised in *Gpr161*$^{mut1/mut1}$ embryos in the neural tube. While Gli2R formation is much less efficient than Gli3R formation, lack of Gpr161 both inside and outside cilia is likely required for preventing Gli2 phosphorylation by PKA. However, *Gpr161* ko cells show Gli2 accumulation in cilia irrespective of pathway activation, and such accumulation persists upon *Gpr161*^{mut1} expression in ko cells. Similar basal accumulation of Gli2 in cilia has also been observed in resting *PKA* null MEFs (Tuson et al., 2011)

and cells lacking Ankmy2 that regulates adenylyl cyclase trafficking to cilia (Somatilaka et al., 2020). Gli2/3 is complexed with Suppressor of Fused (Sufu) and GliR formation requires Gli-Sufu complex (Humke et al., 2010; Kise et al., 2009). Dissociation of Sufu from Gli2/3 is a hallmark of Hh-stimulated signaling by Smo and requires cilia (Humke et al., 2010; Tukachinsky et al., 2010). Gli2 accumulation in cilia in the absence of ciliary Gpr161 pools suggest such accumulation to be upstream of full scale Gli2 activation and probably arises from dissociation from Sufu, but restricted Gli2 phosphorylation is insufficient to cause discernible processing defects.

Gpr161 ciliary pools regulate Hh repression mediated morpho-phenotypic spectrum

Conceptually, the complexity in Hh regulation in tissues by cilia can be simplified based on genetic epistasis between Hh pathway and *Gli2*, *Gli3R* and cilia mutants (Falkenstein & Vokes, 2014; Kopinke et al., 2020). Phenotypes rescued by Gli3R or Gli2 loss are GliR- or Gli2A- dependent, exemplifying tissues regulated primarily by GliA or GliR thresholds, respectively. Phenotypes rescued by both Gli3R or Gli2 loss exemplify tissues that sense ratio between GliA and GliR levels, whereas repression by GliR in absence of Hh expression is a feature of other tissues. Tissues that predominantly require Gli2/Gli3 activation for patterning, such as the ventral neural tube, show lack of activation from loss of cilia. In contrast, tissues that require Gli repressor, such as midface and limbbuds, show lack of repression phenotypes with loss of cilia. Although Gli family members bind to same consensus DNA sequences, the differential roles of GliA and GliR in sculpting tissues could likely arise from context-dependent cis-regulation of targets by co-activators/repressors (Oosterveen et al., 2012). Alternatively, tissue-specific regulation of enhancer activity could regulate Gli-mediated repression (Lex et al., 2020). The effects of ciliary loss of Gpr161 are dependent on requirements of the tissues on GliR levels as follows:

(a) Neural tube. Ventral part of the neural tube is mainly regulated by Gli2 and Gli3 activators (Bai & Joyner, 2001; Bai et al., 2004), whereas intermediate levels of neural tube are regulated by Gli3 repressor levels (Persson et al., 2002). Complete lack of *Gpr161* causes

expansion of the ventral, including ventral-most progenitors rostrocaudally (Mukhopadhyay et al., 2013). However, lack of Gpr161 ciliary pools in *Gpr161*$^{mut1/ko}$ prevent ventral-most progenitor expansion but retains ventral expansion of Nkx6.1 in the intermediate levels of neural tube. Thus, lack of ciliary Gpr161 pools in *Gpr161*$^{mut1/ko}$ prevent sufficient Gli3R processing required to inhibit intermediate level ventralization (**Figure 8A**) and phenocopies *Gpr161; Gli2* double ko. Furthermore, restoration of Gli3R by increased extracellular Gpr161 pools in *Gpr161*$^{mut1/mut1}$ prevents such intermediate level ventralization of Nkx6.1. Lack of the cilia localized GTPase, Arl13b, results in both ventral and dorsal expansion of intermediate Shh-dependent cell fates (Caspary et al., 2007). However, such regulation does not require ciliary pools of Arl13b (Gigante et al., 2020).

Gpr161$^{mut1/ko}$ embryos also show exencephaly and spina bifida, similar to *Gpr161* ko (Mukhopadhyay et al., 2013). Recently, *GPR161* mutations in patients suffering from caudal neural tube defects (spina bifida) have been reported (Kim et al., 2019). While mutants causing Hh pathway hyperactivation are associated with neural tube defects (Murdoch & Copp, 2010; Somatilaka et al., 2020; Ybot-Gonzalez et al., 2002), cross-regulation with other pathways including Wnt (Zhao et al., 2014) and BMP signaling (Ybot-Gonzalez et al., 2007) could determine neural tube closure at different spinal levels. A ciliary retained but PKA-RI non-binding *Gpr161*^{vl} truncation mutant (Bachmann et al., 2016; Pal et al., 2016) is also associated with spina bifida (Matteson et al., 2008), and could involve Wnt signaling defects (Li et al., 2015). Role of ciliary Gpr161 in regulation of these pathways with relation to neural tube closure is presently unclear.

(b) Limb buds. Lack of Gpr161 ciliary pools in both limb buds shows increased Hh pathway targets and expanded *Hoxd13* from lack of Gli3R contributing to polydactyly. We do not see ectopic Shh expression as in *Prx1-Cre; Gpr161*$^{f/f}$ (Hwang et al., 2018); instead, the Shh expression in the posterior limb bud is diffuse, probably from deficient counter-antagonism between Gli3R and dHand (Charite et al., 2000; te Welscher et al., 2002), which drives Shh

expression (Charite et al., 2000). Similarly, a hypomorphic *Ift88* mutant that causes short cilia causes premature expansion of *dHand* before Shh expression suggesting compromised Gli3R formation and preaxial polydactyly without ectopic Shh expression (Liu et al., 2005). Forelimb buds are also completely lacking in *Gpr161*$^{ko/ko}$ embryos (Hwang et al., 2018), unlike in *Gpr161*$^{mut1/ko}$ and *Gpr161*$^{mut1/mut1}$ embryos, presumably from high Hh signaling in the presumptive limb fields in *Gpr161*$^{ko/ko}$. Therefore, the lack of Gpr161 pools in cilia demonstrate effects from moderate levels of derepression of the Hh pathway (**Figure 8B**).

(c) Craniofacial development. Shh is expressed from the frontonasal ectodermal zone (FEZ) in the medial nasal processes (Hu & Marcucio, 2009). Midfacial tissues are regulated by Gli2R and Gli3R levels in normal morphogenesis by preventing midfacial widening (Chang et al., 2016; Schock & Brugmann, 2017). Lack of Gpr161 ciliary pools phenocopies *Gpr161* deletion in cranial neural crest using *Wnt1-Cre* in showing midfacial widening similar to loss of cilia or lack of Gli2 and Gli3 (Brugmann, Allen, et al., 2010; Chang et al., 2016). The facial phenotypes are accompanied by increased levels of *Ptch1* and *Gli1* transcripts in the mid-facial tissues. However, conventional pathway outputs such as *Ptch1* and *Gli1* expression are not increased in the affected tissues upon ciliary loss (Chang et al., 2016), suggesting Hh hyperactivation to be stronger upon *Gpr161* loss from cilia. Cilia regulates both GliA and GliR; therefore, loss of cilia, despite causing lack of repression, might not be as effective in causing pathway hyperactivation as *Gpr161* loss. The craniofacial phenotypes and upregulation of *Ptch1* transcripts persists in mid face of *Gpr161; Gli2* double ko, consistent with derepression from lack of GliR in causing the mid-facial phenotypes (**Figure 8C**).

In conclusion, the results presented here establish a role for Gpr161-mediated cAMP signaling propagated by ciliary and extraciliary compartments in establishing tissue specific GliR thresholds that direct precise morpho-phenotypic outcomes from Hh pathway hyperactivation. By establishing an allelic series for Gpr161-mediated Hh pathway repression, we are also poised to unravel neomorphic phenotypic outcomes from varying signaling strength of Hh signaling.

Materials and Methods

EXPERIMENTAL MODEL AND SUBJECT DETAILS

ES cells

A BAC overlapping the mouse *Gpr161* genomic locus was engineered by recombineering using an FRT-PGKneo-FRT selection cassette. The required mutation (with an engineered NotI site) was separated from the selection cassette by 536 bp (Lee et al., 2001). Recombineering was done by the Biomedical Research Core Facility, University of Michigan (Zeidler et al., 2011). The exon 4 fragments of the *Gpr161*^{mut1} targeting construct were generated using this engineered BAC (#RP23-235-E18) by further cloning into a modified pGKneoloxP2.DTA.2 vector as follows. The pGKneoloxP2.DTA.2 vector was digested with SacII and NheI and religated. The left arm consisting of 4100 bp upstream and the right arm consisting of 4800 bp downstream of the FRT-PGKneo-FRT cassette in the BAC were PCR cloned into the HindIII site of this modified vector (**Figure 2, figure supplement 1**). The engineered plasmid was linearized with XhoI and was electroporated into JM8.N4 ES cells at the Transgenic Core in UT Southwestern, Dallas (Figure 2C). From among 469 ES cell clones, 56 clones were first screened by PCR, and two clones 4D9 and 5F9 were further screened by southern blotting with probes as marked in Figure 2A. ES cells were grown on SNL feeders with media containing 20% Serum, 6 mM L-glutamine, 1X Penicillin/Streptomycin, 1 mM β-mercaptoethanol, 1 mM Non-essential Amino Acids, 1X Nucleosides, 10 mg/L Sodium Pyruvate, ESGRO supplement 66 μl/L and incubated at 37 ^{0}C in 5% CO_2 (Dr. Robert Hammer lab, UT Southwestern, Dallas).

Mouse strains

The *Gpr161*$^{mut1\text{-}neo/+}$ ES cells (5F9 clone) were injected into host embryos of the C57BL/6 albino strain by the transgenic core (Dr. Robert Hammer lab, UT Southwestern Medical Center, Dallas). Mice with germline transmission were crossed with Flp-O (Jackson lab; Stock no: 012930) for deleting the FRT-PGKneo-FRT cassette to generate the *Gpr161*^{mut1} allele. The *Gpr161* knockout and conditional allele targeting the third exon crossed has been described before (Hwang et al., 2018). Double knockout analysis was performed using *Gli2*^{tm1Alj} (ko) allele (Mo et al., 1997). *Prx1-Cre* ((Logan et al., 2002); Jax strain No: 005584) or *Wnt1-Cre* ((Lewis et al., 2013); Jax strain No: 022501) was crossed with the *Gpr161*$^{f/f}$. The *Gli2 ko* and *Gpr161* floxed alleles were linked through genetic recombination by breeding *Gpr161*$^{f/f}$ with *Gli2*$^{ko/+}$ animals. Crossing with CAG-Cre recombinase line (Sakai & Miyazaki, 1997), in which Cre is expressed ubiquitously, generated the linked *Gpr161; Gli2* double knockout allele. Yolk sac DNA was used for genotyping embryos. Mice were housed in standard cages that contained three to five mice per cage, with water and standard diet *ad libitum* and a 12 h light/dark cycle. Noon of the day on which a vaginal plug was found was considered E0.5. All the animals in the study were handled according to protocols approved by the UT Southwestern Institutional Animal Care and Use Committee, and the mouse colonies were maintained in a barrier facility at UT Southwestern, in agreement with the State of Texas legal and ethical standards of animal care.

Cell lines and MEFs

NIH3T3 and RPE hTERT were authenticated by and purchased from ATCC. They have tested negative for Mycoplasma. β-arrestin 1/2 double knockout MEFs were from Robert Lefkowitz and tested negative for Mycoplasma. The *Gpr161* ko NIH 3T3 Flp-In cell line was a gift from Rajat Rohatgi (Pusapati et al., 2018). The cells were cultured in DMEM-high glucose media (D5796; Sigma) with 10% BCS (Sigma-Aldrich), 0.05 mg/ml penicillin, 0.05 mg/ml streptomycin, and 4.5 mM glutamine. Stable knockout cell lines were generated by retroviral infection with pBABE constructs having untagged wild type or mutant *Gpr161* inserts followed by antibiotic selection. RPE hTERT cells were grown in DMEM F12 media with 10% FBS (Sigma-Aldrich), 0.05 mg/ml

penicillin, 0.05 mg/ml streptomycin, and 4.5 mM glutamine. RPE hTert cells were retrovirally infected with C-term LAP-tagged *Gpr161* wild type or mutant constructs and flow sorted for GFP after puromycin selection. Stable doxycycline-inducible NIH 3T3 Tet-on 3G cells expressing untagged *Gpr161* and *Gpr161*^{mut1} receptor variants were generated by retroviral infection. These cell lines were grown in Tet-free serum (Clontech) until induction by Doxycycline (Mukhopadhyay et al., 2013). Single, multiple amino acid mutations, or deletions in full-length Gpr161 were generated using Quikchange site-directed mutagenesis kit (Stratagene or Q5 Mutagenesis Kit (NEB).

METHOD DETAILS

Mouse genotyping

Genotyping of *Gpr161 mut1* alleles were performed using primers in the intron 3-4 (5' CAGAAAGCAACAGCAAAGCA) and intron 4-5 (5' ACCCTGACACTGCCCTTAGC). The PCR product of wild type and *mut1* allele bands was 927 bp, but only the PCR product from the *mut1* allele was digested into 400 and 527 bp products with NotI. Genotyping of *Gpr161* knockout or floxed alleles were performed using primers in the deleted 4th exon (5' CAAGATGGATTCGCAGTAGCTTGG), flanking the 3' end of the deleted exon (5' ATGGGGTACACCATTGGATACAGG), and in the Neo cassette (5' CAACGGGTTCTTCTGTTAGTCC). Wild type, floxed and knockout bands were 816, 965, and 485 bp, respectively (Hwang et al., 2018). *Cre* allele was genotyped with Cre-F (5'-AAT GCT GTC ACT TGG TCG TGG C-3') and Cre-R (5'-GAA AAT GCT TCT GTC CGT TTG C-3') primers (100 bp amplicon). To genotype *Gli2* mice, Gli2 sense (5'-AAA CAA AGC TCC TGT ACA CG-3'), Gli2 antisense (5'-CAC CCC AAA GCA TGT GTT TT-3') and pPNT (5'-ATG CCT GCT CTT TAC TGA AG-3') primers were used. Wild type and knockout bands were 300 bp and 600 bp, respectively.

siRNA transfection

RPE hTERT cells were passaged on glass coverslips and transfected with siRNA using Lipofectamine RNAiMax (Invitrogen). OTP non-targeting pool (GE Healthcare) was used as control siRNAs in all experiments. The siRNA sequences for INPP5E (J-020852-05) is 5′-GGAAUUAAAAGACGGAUUU-3′ and has been validated before (Humbert et al., 2012). The siRNA sequences for BBS4 (D-013649-04) is 5′-CGAUCUGACUUAUAUAAUG-3′ and has been validated before (Loktev et al., 2008). For INPP5E RNAi, 100 nM siRNA was transfected during plating followed by 100 nM reverse transfection 24 h after plating. 72 h after first transfection, the cells were starved with 0.2 % FBS starving media for 24h and fixed in 4% paraformaldehyde (PFA) for immunofluorescence. For *BBS4* RNAi, 100 nM siRNA was reverse transfected 24 h after plating. 48 h after the transfection, the cells were starved with 0.2 % FBS starving media for 24h and fixed in 4% paraformaldehyde (PFA) for immunofluorescence.

TR-FRET cAMP assays

We used a TR-FRET cAMP assay (Cisbio) for estimating cAMP as these assays eliminate the background noise due to FRET-based estimation of signals. Also, the use of long-lived fluorophores (in this case lathanides), combined with time-resolved detection (a delay between excitation and emission detection) minimizes prompt intrinsic fluorescence interferences (Degorce et al., 2009). TR-FRET assays on stable doxycycline-inducible NIH 3T3 Tet-on 3G cells expressing *Gpr161* or *Gpr161*^{mut1} were performed according to manufacturer's instructions (Cisbio) (Mukhopadhyay et al., 2013). Cells were plated on 96 well poly-D-lysine coated plates and induced with doxycycline (2 ug/ml) for 24 hrs. Cells were finally treated with the nonselective phosphodiesterase inhibitor IBMX (1mM). Individual treatments were run in each experiment in triplicate. The final FRET counts were recorded using an EnVision 2103 multiplate reader (Perkin Elmer). cAMP levels (nM) were calculated as interpolated values from a standard curve. Standard

curves were generated using least squares fitting method (with R^2 value >0.99) and values for unknowns were interpolated using Graphpad Prism.

Tissue processing, antibodies, immunostaining and microscopy

Mouse embryos fixed in 4% PFA overnight at 4°C and processed for cryosectioning. For cryosectioning, the embryos were incubated in 30% sucrose at 4°C until they were submerged in the solution. Embryos were mounted with OCT compound. Embryos in OCT were cut into 15 µm frozen sections. The sections were incubated in PBS for 15 min to dissolve away the OCT. Sections were then blocked using blocking buffer (1% normal donkey serum [Jackson immunoResearch, West Grove, PA] in PBS) for 1 h at room temperature. Sections were incubated with primary antibodies against the following antigens; overnight at 4°C: FoxA2 (1:1000, ab108422; Abcam), Nkx6.1 (1:100, F55A10-s; DSHB), Pax6 (1:2000, 901301; Biolegend), Pax7 (1:10; DSHB). After three PBS washes, the sections were incubated in secondary antibodies (Alexa Fluor 488-, 555-, 594-, 647- conjugated secondary antibodies, 1:500; Life Technologies, Carlsbad, CA or Jackson ImmunoResearch) for 1 h at room temperature. Cell nuclei were stained with Hoechst 33342 (Life Technologies). Slides were mounted with Fluoromount-G (0100-01; Southern Biotech) and images were acquired with a Zeiss AxioImager.Z1 microscope. For immunofluorescence experiments in cell lines, cells were cultured on coverslips until confluent and starved for 48 h. To quantify ciliary Gli2 and Gpr161 levels, cells were treated with 500 nM SAG or DMSO for 24 h after 24 h of serum starvation. In some experiments, Transferrin conjugated with Alexa Fluor 568 (Life technologies, T23365) was added (10 µg/ml) in starvation media at 37°C for 30 min before fixation. Cells were fixed with 4% PFA for 10 min at room temperature and postfixed for 5 min with methanol at -20°C for γ-tubulin immunostaining. After blocking with 5% normal donktey serum, the cells were incubated with primary antibody solutions for 1 h at room temperature followed by treatment with secondary antibodies for 30 min along with Hoechst. Primary antibodies used were against Gpr161 (1:200, custom-made) (Pal et al., 2016), acetylated α-tubulin (mAb 6-11B-1, Sigma; 1:2000), GFP (Abcam ab13970), Tulp3 (1:500, gift from Jonathan Eggenschwiler) (Norman et al., 2009), Gli2 (1:500, gift from Jonathan Eggenschwiler) (Cho et al., 2008) , γ-tubulin (GTU-88, Sigma; 1:500). Coverslips were mounted with Fluoromount-G and images were acquired with a Zeiss AxioImager.Z1 microscope using a 40 × oil immersion objective lens.

Reverse transcription, quantitative PCR.

RNA was extracted using the GenElute mammalian total RNA purification kit (RTN350; Sigma). Genomic DNA was eliminated by DNase I (D5307; Sigma). qRT-PCR was performed with SYBR Green Quantitative RT-qPCR Kit (QR0100; Sigma) or Kicqstart One-Step Probe RT-qPCR ReadyMix (KCQS07; Sigma). *Gli1* (Wen et al., 2010) and *Ptch2* (Somatilaka et al., 2020) TaqMan probes for qRT-PCR were published before. Inventoried probes for *Gpr161*, and *Gapdh* were from Applied Biosystems. Reactions were run in CFX96 Real time System (Bio Rad).

Gli1/2/3 immunoblotting.

Embryos or limb buds were processed for Gli1/2/3 immunoblotting as described previously (Wen et al., 2010), using Gli3 (AF3690, R&D, 1ug/ml), Gli2 (AF3635, R&D, 1ug/ml), Gli1 (L42B10, Cell Signaling; 1:1000) and α-tubulin (clone DM1A, T6199, Sigma; 1:5000) antibodies. Secondary antibodies tagged with IRDye 680RD and IRDye 800CW for immunoblotting were from LI-COR Biosciences. Levels of Gli proteins were normalized to α-tubulin. 30 ug of lysates were used in immunoblotting, well within the linear range of detection of α-tubulin levels using the DM1A monoclonal antibody and using LI-COR infrared laser-based detection.

GPCR tandem affinity purifications.

MEFs stably expressing LAP tagged Gpr161 variants were lysed in buffer containing 50 mM Tris-HCl, pH 7.4, 200 mM KCl, 1 mM MgCl2, 1mM EGTA, 10 % glycerol, 1 mM DTT, 1% digitonin, 0.05% n-Dodecyl-β-D-Maltoside, 0.25% Cholesteryl hemisuccinate, 1 mM of AEBSF, 0.01 mg/mL of Leupeptin, pepstatin and chymostatin (Pal et al., 2015). Lysates were centrifuged at 12000xg for 10 min followed by tandem IPs (Cheeseman & Desai, 2005). Briefly, the GFP immunoprecipitates were first digested with TEV (N terminal LAP) or PreScission (for C terminal LAP) protease for 16 h at 4°C. The supernatants were subjected to secondary IPs with S-protein agarose. The resulting secondary IPs were eluted in 2× urea sample buffer (4 M urea, 4% SDS, 100 mM Tris, pH 6.8, 0.2% bromophenol blue, 20% glycerol, and 200 mM DTT) at 37°C for 30 min and analyzed by immunoblotting (Pal et al., 2015). Tandem-IPs were run on 4–20% Mini-PROTEAN TGX Precast Protein Gels (Bio-Rad). Immunoblots from tandem affinity purifications were probed with antibodies against S-tag (mouse monoclonal MAC112; EMD Millipore) followed by visualization using IRDye-tagged secondary antibodies.

In situ hybridization (ISH)

Antisense riboprobes were made using the following templates: *Ptch1, Gli1, Shh,* (gifts from Andrew McMahon lab and Deanna Grant, Andrew Peterson lab), *Sox9*, *Col2a1* (from Steven Vokes lab, UT Austin), *Hoxd13* (from Xin Sun lab, University of Wisconsin, Madison). Whole mount in situ hybridization using digoxigenin-labeled probes was performed on embryos using standard protocols. Images were acquired using a Leica stereomicroscope (M165 C) with digital camera (DFC500) or Zeiss stereomicroscope (Discovery.V12) and AxioCam MRc.

QUANTIFICATION AND STATISTICAL ANALYSIS

Cilia positive for acetylated α-tubulin and GPR161/TULP3 were counted and expressed as % of GPR161/TULP3 positive cilia. To quantify ciliary pools of GPR161, TULP3, GFP, fluorescence levels were measured using the “Measure” tool of Fiji software. Fluorescence levels of neighboring background areas were subtracted from that of the selected ciliary areas and expressed as corrected fluorescence. Quantification of dorsoventral extent of Nkx6.1 expression to that of the neural tube was done by averaging from 2 or more sections at thoracic region from 2-4 embryos. Statistical analyses were performed using Student’s *t*-test for comparing two groups using GraphPad Prism.

Acknowledgements

This paper is dedicated to the memory of Kathryn Anderson, who has been a constant source of encouragement and inspiration in our studies on ciliary signaling. This project was funded by Alex's Lemonade Foundation (A-grant to S.M.), and National Institutes of Health (1R01GM113023 to SM). We thank UT Southwestern transgenic and mouse animal care facility. We are thankful for kind gifts of reagents from Rajat Rohatgi, Robert Lefkowitz, Jonathan Eggenschwiler, Andrew McMahon, Deanna Grant, Andrew Peterson, Steven Vokes and Xin Sun. We thank Mukhopadhyay lab members for comments on the manuscript. Monoclonal antibodies developed by O. D. Madsen (Nkx6.1) and A. Kawakami (Pax7) were obtained from the Developmental Studies Hybridoma Bank developed under the auspices of the NICHD and maintained by the Department of Biological Sciences, the University of Iowa, Iowa City IA 52242, USA.

Author contributions

S. H. and S. M conceived the project, designed experiments, analyzed most of the data, and wrote the paper with inputs from all authors. S. H. performed most of the experiments. B. N. S. and K. W. performed cryosectioning and immunofluorescence experiments.

Competing Financial Interest Statement

The authors have no competing financial interests to declare.

References

Anvarian, Z., Mykytyn, K., Mukhopadhyay, S., Pedersen, L. B., & Christensen, S. T. (2019, Apr). Cellular signalling by primary cilia in development, organ function and disease. *Nat Rev Nephrol, 15*(4), 199-219. https://doi.org/10.1038/s41581-019-0116-9

Bachmann, V. A., Mayrhofer, J. E., Ilouz, R., Tschaikner, P., Raffeiner, P., Rock, R., Courcelles, M., Apelt, F., Lu, T. W., Baillie, G. S., Thibault, P., Aanstad, P., Stelzl, U., Taylor, S. S., & Stefan, E. (2016, Jul 12). Gpr161 anchoring of PKA consolidates GPCR and cAMP signaling. *Proc Natl Acad Sci U S A, 113*(28), 7786-7791. https://doi.org/10.1073/pnas.1608061113

Badgandi, H. B., Hwang, S. H., Shimada, I. S., Loriot, E., & Mukhopadhyay, S. (2017, Mar 6). Tubby family proteins are adapters for ciliary trafficking of integral membrane proteins. *J Cell Biol, 216*(3), 743-760. https://doi.org/10.1083/jcb.201607095

Bai, C. B., & Joyner, A. L. (2001, Dec). Gli1 can rescue the in vivo function of Gli2. *Development, 128*(24), 5161-5172. https://www.ncbi.nlm.nih.gov/pubmed/11748151

Bai, C. B., Stephen, D., & Joyner, A. L. (2004, Jan). All mouse ventral spinal cord patterning by hedgehog is Gli dependent and involves an activator function of Gli3. *Dev Cell, 6*(1), 103-115. https://doi.org/10.1016/s1534-5807(03)00394-0

Barzi, M., Berenguer, J., Menendez, A., Alvarez-Rodriguez, R., & Pons, S. (2010, Jan 1). Sonic-hedgehog-mediated proliferation requires the localization of PKA to the cilium base. *J Cell Sci, 123*(Pt 1), 62-69. https://doi.org/10.1242/jcs.060020

Bock, A., Annibale, P., Konrad, C., Hannawacker, A., Anton, S. E., Maiellaro, I., Zabel, U., Sivaramakrishnan, S., Falcke, M., & Lohse, M. J. (2020, Sep 17). Optical Mapping of cAMP Signaling at the Nanometer Scale. *Cell, 182*(6), 1519-1530 e1517. https://doi.org/10.1016/j.cell.2020.07.035

Briscoe, J., & Therond, P. P. (2013, Jul). The mechanisms of Hedgehog signalling and its roles in development and disease. *Nat Rev Mol Cell Biol, 14*(7), 416-429. https://doi.org/10.1038/nrm3598

Brugmann, S. A., Allen, N. C., James, A. W., Mekonnen, Z., Madan, E., & Helms, J. A. (2010, Apr 15). A primary cilia-dependent etiology for midline facial disorders. *Hum Mol Genet, 19*(8), 1577-1592. https://doi.org/10.1093/hmg/ddq030

Brugmann, S. A., Cordero, D. R., & Helms, J. A. (2010, Dec). Craniofacial ciliopathies: A new classification for craniofacial disorders. *Am J Med Genet A, 152A*(12), 2995-3006. https://doi.org/10.1002/ajmg.a.33727

Calebiro, D., Nikolaev, V. O., Gagliani, M. C., de Filippis, T., Dees, C., Tacchetti, C., Persani, L., & Lohse, M. J. (2009, Aug). Persistent cAMP-signals triggered by internalized G-protein-coupled receptors. *PLoS Biol, 7*(8), e1000172. https://doi.org/10.1371/journal.pbio.1000172

Caspary, T., Larkins, C. E., & Anderson, K. V. (2007, May). The graded response to Sonic Hedgehog depends on cilia architecture. *Dev Cell, 12*(5), 767-778. https://doi.org/10.1016/j.devcel.2007.03.004

Chang, C. F., Chang, Y. T., Millington, G., & Brugmann, S. A. (2016, Nov). Craniofacial Ciliopathies Reveal Specific Requirements for GLI Proteins during Development of the Facial Midline. *PLoS Genet, 12*(11), e1006351. https://doi.org/10.1371/journal.pgen.1006351

Charite, J., McFadden, D. G., & Olson, E. N. (2000, Jun). The bHLH transcription factor dHAND controls Sonic hedgehog expression and establishment of the zone of polarizing activity during limb development. *Development, 127*(11), 2461-2470. https://www.ncbi.nlm.nih.gov/pubmed/10804186

Chavez, M., Ena, S., Van Sande, J., de Kerchove d'Exaerde, A., Schurmans, S., & Schiffmann, S. N. (2015, Aug 10). Modulation of Ciliary Phosphoinositide Content Regulates Trafficking and Sonic Hedgehog Signaling Output. *Dev Cell, 34*(3), 338-350. https://doi.org/10.1016/j.devcel.2015.06.016

Cheeseman, I. M., & Desai, A. (2005, Jan 11). A combined approach for the localization and tandem affinity purification of protein complexes from metazoans. *Sci STKE, 2005*(266), pl1. https://doi.org/10.1126/stke.2662005pl1

Chen, M. H., Wilson, C. W., Li, Y. J., Law, K. K., Lu, C. S., Gacayan, R., Zhang, X., Hui, C. C., & Chuang, P. T. (2009, Aug 15). Cilium-independent regulation of Gli protein function by Sufu in Hedgehog signaling is evolutionarily conserved. *Genes Dev, 23*(16), 1910-1928. https://doi.org/23/16/1910 [pii]
10.1101/gad.1794109

Cho, A., Ko, H. W., & Eggenschwiler, J. T. (2008, Sep 1). FKBP8 cell-autonomously controls neural tube patterning through a Gli2- and Kif3a-dependent mechanism. *Dev Biol, 321*(1), 27-39. https://doi.org/10.1016/j.ydbio.2008.05.558

Corbit, K. C., Aanstad, P., Singla, V., Norman, A. R., Stainier, D. Y., & Reiter, J. F. (2005, Oct 13). Vertebrate Smoothened functions at the primary cilium. *Nature, 437*(7061), 1018-1021. https://doi.org/10.1038/nature04117

Crilly, S. E., & Puthenveedu, M. A. (2020, Nov 24). Compartmentalized GPCR Signaling from Intracellular Membranes. *J Membr Biol*. https://doi.org/10.1007/s00232-020-00158-7

Degorce, F., Card, A., Soh, S., Trinquet, E., Knapik, G. P., & Xie, B. (2009). HTRF: A technology tailored for drug discovery - a review of theoretical aspects and recent applications. *Curr Chem Genomics, 3*, 22-32. https://doi.org/10.2174/1875397300903010022

Delling, M., Indzhykulian, A. A., Liu, X., Li, Y., Xie, T., Corey, D. P., & Clapham, D. E. (2016, Mar 31). Primary cilia are not calcium-responsive mechanosensors. *Nature, 531*(7596), 656-660. https://doi.org/10.1038/nature17426

Dessaud, E., McMahon, A. P., & Briscoe, J. (2008, Aug). Pattern formation in the vertebrate neural tube: a sonic hedgehog morphogen-regulated transcriptional network. *Development, 135*(15), 2489-2503. https://doi.org/10.1242/dev.009324

Falkenstein, K. N., & Vokes, S. A. (2014, Sep). Transcriptional regulation of graded Hedgehog signaling. *Semin Cell Dev Biol, 33*, 73-80. https://doi.org/10.1016/j.semcdb.2014.05.010

Gabriel, G. C., Young, C. B., & Lo, C. W. (2020, May 14). Role of cilia in the pathogenesis of congenital heart disease. *Semin Cell Dev Biol*. https://doi.org/10.1016/j.semcdb.2020.04.017

Garcia-Gonzalo, F. R., Corbit, K. C., Sirerol-Piquer, M. S., Ramaswami, G., Otto, E. A., Noriega, T. R., Seol, A. D., Robinson, J. F., Bennett, C. L., Josifova, D. J., Garcia-Verdugo, J. M., Katsanis, N., Hildebrandt, F., & Reiter, J. F. (2011, Jul 3). A transition zone complex regulates mammalian ciliogenesis and ciliary membrane composition. *Nat Genet, 43*(8), 776-784. https://doi.org/10.1038/ng.891

Gigante, E. D., Taylor, M. R., Ivanova, A. A., Kahn, R. A., & Caspary, T. (2020, Mar 4). ARL13B regulates Sonic hedgehog signaling from outside primary cilia. *Elife, 9*. https://doi.org/10.7554/eLife.50434

Goetz, S. C., & Anderson, K. V. (2010, May). The primary cilium: a signalling centre during vertebrate development. *Nat Rev Genet, 11*(5), 331-344. https://doi.org/10.1038/nrg2774

Guo, J., Otis, J. M., Suciu, S. K., Catalano, C., Xing, L., Constable, S., Wachten, D., Gupton, S., Lee, J., Lee, A., Blackley, K. H., Ptacek, T., Simon, J. M., Schurmans, S., Stuber, G. D., Caspary, T., & Anton, E. S. (2019, Dec 16). Primary Cilia Signaling Promotes Axonal Tract Development and Is Disrupted in Joubert Syndrome-Related Disorders Models. *Dev Cell, 51*(6), 759-774 e755. https://doi.org/10.1016/j.devcel.2019.11.005

Hansen, J. N., Kaiser, F., Klausen, C., Stuven, B., Chong, R., Bonigk, W., Mick, D. U., Moglich, A., Jurisch-Yaksi, N., Schmidt, F. I., & Wachten, D. (2020, Jun 24). Nanobody-directed targeting of optogenetic tools to study signaling in the primary cilium. *Elife, 9*. https://doi.org/10.7554/eLife.57907

Haycraft, C. J., Banizs, B., Aydin-Son, Y., Zhang, Q., Michaud, E. J., & Yoder, B. K. (2005, Oct). Gli2 and Gli3 localize to cilia and require the intraflagellar transport protein polaris for processing and function. *PLoS Genet, 1*(4), e53. https://doi.org/10.1371/journal.pgen.0010053

Hu, D., & Marcucio, R. S. (2009, Jan 1). Unique organization of the frontonasal ectodermal zone in birds and mammals. *Dev Biol, 325*(1), 200-210. https://doi.org/10.1016/j.ydbio.2008.10.026

Huangfu, D., Liu, A., Rakeman, A. S., Murcia, N. S., Niswander, L., & Anderson, K. V. (2003, Nov 6). Hedgehog signalling in the mouse requires intraflagellar transport proteins. *Nature, 426*(6962), 83-87. https://doi.org/10.1038/nature02061

Huber, C., & Cormier-Daire, V. (2012, Aug 15). Ciliary disorder of the skeleton. *Am J Med Genet C Semin Med Genet, 160C*(3), 165-174. https://doi.org/10.1002/ajmg.c.31336

Hui, C. C., & Angers, S. (2011). Gli proteins in development and disease. *Annu Rev Cell Dev Biol, 27*, 513-537. https://doi.org/10.1146/annurev-cellbio-092910-154048

Humke, E. W., Dorn, K. V., Milenkovic, L., Scott, M. P., & Rohatgi, R. (2010, Apr 1). The output of Hedgehog signaling is controlled by the dynamic association between Suppressor of Fused and the Gli proteins. *Genes Dev, 24*(7), 670-682. https://doi.org/24/7/670 [pii] 10.1101/gad.1902910

Hwang, S. H., White, K. A., Somatilaka, B. N., Shelton, J. M., Richardson, J. A., & Mukhopadhyay, S. (2018, Jan 8). The G protein-coupled receptor Gpr161 regulates forelimb formation, limb patterning and skeletal morphogenesis in a primary cilium-dependent manner. *Development, 145*(1). https://doi.org/10.1242/dev.154054

Irannejad, R., Tomshine, J. C., Tomshine, J. R., Chevalier, M., Mahoney, J. P., Steyaert, J., Rasmussen, S. G., Sunahara, R. K., El-Samad, H., Huang, B., & von Zastrow, M. (2013,

Mar 28). Conformational biosensors reveal GPCR signalling from endosomes. *Nature, 495*(7442), 534-538. https://doi.org/10.1038/nature12000

Jia, J., Kolterud, A., Zeng, H., Hoover, A., Teglund, S., Toftgard, R., & Liu, A. (2009, Jun 15). Suppressor of Fused inhibits mammalian Hedgehog signaling in the absence of cilia. *Dev Biol, 330*(2), 452-460. https://doi.org/S0012-1606(09)00241-3 [pii] 10.1016/j.ydbio.2009.04.009

Jiang, J. Y., Falcone, J. L., Curci, S., & Hofer, A. M. (2019, Jun 11). Direct visualization of cAMP signaling in primary cilia reveals up-regulation of ciliary GPCR activity following Hedgehog activation. *Proc Natl Acad Sci U S A, 116*(24), 12066-12071. https://doi.org/10.1073/pnas.1819730116

Kim, J., Kato, M., & Beachy, P. A. (2009, Dec 22). Gli2 trafficking links Hedgehog-dependent activation of Smoothened in the primary cilium to transcriptional activation in the nucleus. *Proc Natl Acad Sci U S A, 106*(51), 21666-21671. https://doi.org/10.1073/pnas.0912180106

Kim, S. E., Lei, Y., Hwang, S. H., Wlodarczyk, B. J., Mukhopadhyay, S., Shaw, G. M., Ross, M. E., & Finnell, R. H. (2019, Jan 15). Dominant negative GPR161 rare variants are risk factors of human spina bifida. *Hum Mol Genet, 28*(2), 200-208. https://doi.org/10.1093/hmg/ddy339

Kise, Y., Morinaka, A., Teglund, S., & Miki, H. (2009, Sep 25). Sufu recruits GSK3beta for efficient processing of Gli3. *Biochem Biophys Res Commun, 387*(3), 569-574. https://doi.org/10.1016/j.bbrc.2009.07.087

Kopinke, D., Norris, A. M., & Mukhopadhyay, S. (2020, Jun 12). Developmental and regenerative paradigms of cilia regulated hedgehog signaling. *Semin Cell Dev Biol*. https://doi.org/10.1016/j.semcdb.2020.05.029

Kotowski, S. J., Hopf, F. W., Seif, T., Bonci, A., & von Zastrow, M. (2011, Jul 28). Endocytosis promotes rapid dopaminergic signaling. *Neuron, 71*(2), 278-290. https://doi.org/10.1016/j.neuron.2011.05.036

Kovacs, J. J., Whalen, E. J., Liu, R., Xiao, K., Kim, J., Chen, M., Wang, J., Chen, W., & Lefkowitz, R. J. (2008, Jun 27). Beta-arrestin-mediated localization of smoothened to the primary cilium. *Science, 320*(5884), 1777-1781. https://doi.org/10.1126/science.1157983

Lee, E. C., Yu, D., Martinez de Velasco, J., Tessarollo, L., Swing, D. A., Court, D. L., Jenkins, N. A., & Copeland, N. G. (2001, Apr 1). A highly efficient Escherichia coli-based

chromosome engineering system adapted for recombinogenic targeting and subcloning of BAC DNA. *Genomics, 73*(1), 56-65. https://doi.org/10.1006/geno.2000.6451

Leurs, R., Smit, M. J., Alewijnse, A. E., & Timmerman, H. (1998, Nov). Agonist-independent regulation of constitutively active G-protein-coupled receptors. *Trends Biochem Sci, 23*(11), 418-422. https://doi.org/S0968-0004(98)01287-0 [pii]

Lewis, A. E., Vasudevan, H. N., O'Neill, A. K., Soriano, P., & Bush, J. O. (2013, Jul 15). The widely used Wnt1-Cre transgene causes developmental phenotypes by ectopic activation of Wnt signaling. *Dev Biol, 379*(2), 229-234. https://doi.org/10.1016/j.ydbio.2013.04.026

Lex, R. K., Ji, Z., Falkenstein, K. N., Zhou, W., Henry, J. L., Ji, H., & Vokes, S. A. (2020, Jan 28). GLI transcriptional repression regulates tissue-specific enhancer activity in response to Hedgehog signaling. *Elife, 9*. https://doi.org/10.7554/eLife.50670

Li, B. I., Matteson, P. G., Ababon, M. F., Nato, A. Q., Jr., Lin, Y., Nanda, V., Matise, T. C., & Millonig, J. H. (2015, Jun 1). The orphan GPCR, Gpr161, regulates the retinoic acid and canonical Wnt pathways during neurulation. *Dev Biol, 402*(1), 17-31. https://doi.org/10.1016/j.ydbio.2015.02.007

Liu, A., Wang, B., & Niswander, L. A. (2005, Jul). Mouse intraflagellar transport proteins regulate both the activator and repressor functions of Gli transcription factors. *Development, 132*(13), 3103-3111. https://doi.org/10.1242/dev.01894

Liu, J., Zeng, H., & Liu, A. (2015, May 1). The loss of Hh responsiveness by a non-ciliary Gli2 variant. *Development, 142*(9), 1651-1660. https://doi.org/10.1242/dev.119669

Logan, M., Martin, J. F., Nagy, A., Lobe, C., Olson, E. N., & Tabin, C. J. (2002, Jun). Expression of Cre Recombinase in the developing mouse limb bud driven by a Prxl enhancer. *Genesis, 33*(2), 77-80. https://doi.org/10.1002/gene.10092

Loktev, A. V., Zhang, Q., Beck, J. S., Searby, C. C., Scheetz, T. E., Bazan, J. F., Slusarski, D. C., Sheffield, V. C., Jackson, P. K., & Nachury, M. V. (2008, Dec). A BBSome subunit links ciliogenesis, microtubule stability, and acetylation. *Dev Cell, 15*(6), 854-865. https://doi.org/10.1016/j.devcel.2008.11.001

Matteson, P. G., Desai, J., Korstanje, R., Lazar, G., Borsuk, T. E., Rollins, J., Kadambi, S., Joseph, J., Rahman, T., Wink, J., Benayed, R., Paigen, B., & Millonig, J. H. (2008, Feb 12). The orphan G protein-coupled receptor, Gpr161, encodes the vacuolated lens locus and controls neurulation and lens development. *Proc Natl Acad Sci U S A, 105*(6), 2088-2093. https://doi.org/10.1073/pnas.0705657105

May, E. A., Kalocsay, M., D'Auriac, I. G., Schuster, P. S., Gygi, S. P., Nachury, M. V., & Mick, D. U. (2021, May 3). Time-resolved proteomics profiling of the ciliary Hedgehog response. *J Cell Biol, 220*(5). https://doi.org/10.1083/jcb.202007207

Mick, D. U., Rodrigues, R. B., Leib, R. D., Adams, C. M., Chien, A. S., Gygi, S. P., & Nachury, M. V. (2015, Nov 23). Proteomics of Primary Cilia by Proximity Labeling. *Dev Cell, 35*(4), 497-512. https://doi.org/10.1016/j.devcel.2015.10.015

Mo, G. C., Ross, B., Hertel, F., Manna, P., Yang, X., Greenwald, E., Booth, C., Plummer, A. M., Tenner, B., Chen, Z., Wang, Y., Kennedy, E. J., Cole, P. A., Fleming, K. G., Palmer, A., Jimenez, R., Xiao, J., Dedecker, P., & Zhang, J. (2017, Apr). Genetically encoded biosensors for visualizing live-cell biochemical activity at super-resolution. *Nat Methods, 14*(4), 427-434. https://doi.org/10.1038/nmeth.4221

Mo, R., Freer, A. M., Zinyk, D. L., Crackower, M. A., Michaud, J., Heng, H. H., Chik, K. W., Shi, X. M., Tsui, L. C., Cheng, S. H., Joyner, A. L., & Hui, C. (1997, Jan). Specific and redundant functions of Gli2 and Gli3 zinc finger genes in skeletal patterning and development. *Development, 124*(1), 113-123. https://www.ncbi.nlm.nih.gov/pubmed/9006072

Moore, B. S., Stepanchick, A. N., Tewson, P. H., Hartle, C. M., Zhang, J., Quinn, A. M., Hughes, T. E., & Mirshahi, T. (2016, Nov 15). Cilia have high cAMP levels that are inhibited by Sonic Hedgehog-regulated calcium dynamics. *Proc Natl Acad Sci U S A, 113*(46), 13069-13074. https://doi.org/10.1073/pnas.1602393113

Mukhopadhyay, S., Badgandi, H. B., Hwang, S. H., Somatilaka, B., Shimada, I. S., & Pal, K. (2017, Jan 15). Trafficking to the primary cilium membrane. *Mol Biol Cell, 28*(2), 233-239. https://doi.org/10.1091/mbc.E16-07-0505

Mukhopadhyay, S., & Rohatgi, R. (2014, Sep). G-protein-coupled receptors, Hedgehog signaling and primary cilia. *Semin Cell Dev Biol, 33*, 63-72. https://doi.org/10.1016/j.semcdb.2014.05.002

Mukhopadhyay, S., Wen, X., Chih, B., Nelson, C. D., Lane, W. S., Scales, S. J., & Jackson, P. K. (2010, Oct 1). TULP3 bridges the IFT-A complex and membrane phosphoinositides to promote trafficking of G protein-coupled receptors into primary cilia. *Genes Dev, 24*(19), 2180-2193. https://doi.org/10.1101/gad.1966210

Mukhopadhyay, S., Wen, X., Ratti, N., Loktev, A., Rangell, L., Scales, S. J., & Jackson, P. K. (2013, Jan 17). The ciliary G-protein-coupled receptor Gpr161 negatively regulates the

Sonic hedgehog pathway via cAMP signaling. *Cell, 152*(1-2), 210-223. https://doi.org/10.1016/j.cell.2012.12.026

Murdoch, J. N., & Copp, A. J. (2010, Aug). The relationship between sonic Hedgehog signaling, cilia, and neural tube defects. *Birth Defects Res A Clin Mol Teratol, 88*(8), 633-652. https://doi.org/10.1002/bdra.20686

Nachury, M. V., & Mick, D. U. (2019, Jul). Establishing and regulating the composition of cilia for signal transduction. *Nat Rev Mol Cell Biol, 20*(7), 389-405. https://doi.org/10.1038/s41580-019-0116-4

Niewiadomski, P., Kong, J. H., Ahrends, R., Ma, Y., Humke, E. W., Khan, S., Teruel, M. N., Novitch, B. G., & Rohatgi, R. (2014, Jan 16). Gli protein activity is controlled by multisite phosphorylation in vertebrate Hedgehog signaling. *Cell Rep, 6*(1), 168-181. https://doi.org/10.1016/j.celrep.2013.12.003

Niswander, L. (2003, Feb). Pattern formation: old models out on a limb. *Nat Rev Genet, 4*(2), 133-143. https://doi.org/10.1038/nrg1001

Norman, R. X., Ko, H. W., Huang, V., Eun, C. M., Abler, L. L., Zhang, Z., Sun, X., & Eggenschwiler, J. T. (2009, May 15). Tubby-like protein 3 (TULP3) regulates patterning in the mouse embryo through inhibition of Hedgehog signaling. *Hum Mol Genet, 18*(10), 1740-1754. https://doi.org/10.1093/hmg/ddp113

Nozaki, S., Katoh, Y., Kobayashi, T., & Nakayama, K. (2018). BBS1 is involved in retrograde trafficking of ciliary GPCRs in the context of the BBSome complex. *PLoS One, 13*(3), e0195005. https://doi.org/10.1371/journal.pone.0195005

Oosterveen, T., Kurdija, S., Alekseenko, Z., Uhde, C. W., Bergsland, M., Sandberg, M., Andersson, E., Dias, J. M., Muhr, J., & Ericson, J. (2012, Nov 13). Mechanistic differences in the transcriptional interpretation of local and long-range Shh morphogen signaling. *Dev Cell, 23*(5), 1006-1019. https://doi.org/10.1016/j.devcel.2012.09.015

Pal, K., Badgandi, H., & Mukhopadhyay, S. (2015). Studying G protein-coupled receptors: immunoblotting, immunoprecipitation, phosphorylation, surface labeling, and cross-linking protocols. *Methods Cell Biol, 127*, 303-322. https://doi.org/10.1016/bs.mcb.2014.12.003

Pal, K., Hwang, S. H., Somatilaka, B., Badgandi, H., Jackson, P. K., DeFea, K., & Mukhopadhyay, S. (2016, Mar 28). Smoothened determines beta-arrestin-mediated removal of the G protein-coupled receptor Gpr161 from the primary cilium. *J Cell Biol, 212*(7), 861-875. https://doi.org/10.1083/jcb.201506132

Pan, Y., Bai, C. B., Joyner, A. L., & Wang, B. (2006, May). Sonic hedgehog signaling regulates Gli2 transcriptional activity by suppressing its processing and degradation. *Mol Cell Biol, 26*(9), 3365-3377. https://doi.org/10.1128/MCB.26.9.3365-3377.2006

Persson, M., Stamataki, D., te Welscher, P., Andersson, E., Bose, J., Ruther, U., Ericson, J., & Briscoe, J. (2002, Nov 15). Dorsal-ventral patterning of the spinal cord requires Gli3 transcriptional repressor activity. *Genes Dev, 16*(22), 2865-2878. https://doi.org/10.1101/gad.243402

Pusapati, G. V., Kong, J. H., Patel, B. B., Gouti, M., Sagner, A., Sircar, R., Luchetti, G., Ingham, P. W., Briscoe, J., & Rohatgi, R. (2018). G protein–coupled receptors control the sensitivity of cells to the morphogen Sonic Hedgehog. *Science Signaling, 11*(516), eaao5749. https://doi.org/10.1126/scisignal.aao5749

Reiter, J. F., & Leroux, M. R. (2017, Sep). Genes and molecular pathways underpinning ciliopathies. *Nat Rev Mol Cell Biol, 18*(9), 533-547. https://doi.org/10.1038/nrm.2017.60

Rohatgi, R., Milenkovic, L., & Scott, M. P. (2007, Jul 20). Patched1 regulates hedgehog signaling at the primary cilium. *Science, 317*(5836), 372-376. https://doi.org/10.1126/science.1139740

Saade, M., Gonzalez-Gobartt, E., Escalona, R., Usieto, S., & Marti, E. (2017, Apr 27). Shh-mediated centrosomal recruitment of PKA promotes symmetric proliferative neuroepithelial cell division. *Nat Cell Biol, 19*(5), 493-503. https://doi.org/10.1038/ncb3512

Sakai, K., & Miyazaki, J. (1997, Aug 18). A transgenic mouse line that retains Cre recombinase activity in mature oocytes irrespective of the cre transgene transmission. *Biochem Biophys Res Commun, 237*(2), 318-324. https://doi.org/10.1006/bbrc.1997.7111

Schock, E. N., & Brugmann, S. A. (2017, Sep 1). Discovery, Diagnosis, and Etiology of Craniofacial Ciliopathies. *Cold Spring Harb Perspect Biol, 9*(9). https://doi.org/10.1101/cshperspect.a028258

Seifert, R., & Wenzel-Seifert, K. (2002, Nov). Constitutive activity of G-protein-coupled receptors: cause of disease and common property of wild-type receptors. *Naunyn Schmiedebergs Arch Pharmacol, 366*(5), 381-416. https://doi.org/10.1007/s00210-002-0588-0

Shimada, I. S., Hwang, S. H., Somatilaka, B. N., Wang, X., Skowron, P., Kim, J., Kim, M., Shelton, J. M., Rajaram, V., Xuan, Z., Taylor, M. D., & Mukhopadhyay, S. (2018, Jan 30). Basal Suppression of the Sonic Hedgehog Pathway by the G-Protein-Coupled Receptor Gpr161 Restricts Medulloblastoma Pathogenesis. *Cell Rep, 22*(5), 1169-1184. https://doi.org/10.1016/j.celrep.2018.01.018

Shimada, I. S., Somatilaka, B. N., Hwang, S. H., Anderson, A. G., Shelton, J. M., Rajaram, V., Konopka, G., & Mukhopadhyay, S. (2019, Jun 1). Derepression of sonic hedgehog signaling upon Gpr161 deletion unravels forebrain and ventricular abnormalities. *Dev Biol, 450*(1), 47-62. https://doi.org/10.1016/j.ydbio.2019.03.011

Smith, F. D., Esseltine, J. L., Nygren, P. J., Veesler, D., Byrne, D. P., Vonderach, M., Strashnov, I., Eyers, C. E., Eyers, P. A., Langeberg, L. K., & Scott, J. D. (2017, Jun 23). Local protein kinase A action proceeds through intact holoenzymes. *Science, 356*(6344), 1288-1293. https://doi.org/10.1126/science.aaj1669

Somatilaka, B. N., Hwang, S. H., Palicharla, V. R., White, K. A., Badgandi, H., Shelton, J. M., & Mukhopadhyay, S. (2020, Sep 28). Ankmy2 Prevents Smoothened-Independent Hyperactivation of the Hedgehog Pathway via Cilia-Regulated Adenylyl Cyclase Signaling. *Dev Cell, 54*(6), 710-726 e718. https://doi.org/10.1016/j.devcel.2020.06.034

te Welscher, P., Fernandez-Teran, M., Ros, M. A., & Zeller, R. (2002, Feb 15). Mutual genetic antagonism involving GLI3 and dHAND prepatterns the vertebrate limb bud mesenchyme prior to SHH signaling. *Genes Dev, 16*(4), 421-426. https://doi.org/10.1101/gad.219202

Tempe, D., Casas, M., Karaz, S., Blanchet-Tournier, M. F., & Concordet, J. P. (2006, Jun). Multisite protein kinase A and glycogen synthase kinase 3beta phosphorylation leads to Gli3 ubiquitination by SCFbetaTrCP. *Mol Cell Biol, 26*(11), 4316-4326. https://doi.org/10.1128/MCB.02183-05

Truong, M. E., Bilekova, S., Choksi, S. P., Li, W., Bugaj, L. J., Xu, K., & Reiter, J. F. (2021, Apr 27). Vertebrate cells differentially interpret ciliary and extraciliary cAMP. *Cell*. https://doi.org/10.1016/j.cell.2021.04.002

Tschaikner, P., Regele, D., Salvenmoser, W., Geley, S., Stefan, E., & Aanstad, P. (2019). Zebrafish GPR161 Contributes to Basal Hedgehog Repression in a Tissue-specific Manner. *bioRxiv*, 616482. https://doi.org/10.1101/616482

Tschaikner, P. M., Regele, D., Rock, R., Salvenmoser, W., Meyer, D., Bouvier, M., Geley, S., Stefan, E., & Aanstad, P. (2021, Feb 17). Feedback control of the Gpr161-Galphas-PKA axis contributes to basal Hedgehog repression in zebrafish. *Development, 148*(4). https://doi.org/10.1242/dev.192443

Tukachinsky, H., Lopez, L. V., & Salic, A. (2010, Oct 18). A mechanism for vertebrate Hedgehog signaling: recruitment to cilia and dissociation of SuFu-Gli protein complexes. *J Cell Biol, 191*(2), 415-428. https://doi.org/10.1083/jcb.201004108

Tuson, M., He, M., & Anderson, K. V. (2011, Nov). Protein kinase A acts at the basal body of the primary cilium to prevent Gli2 activation and ventralization of the mouse neural tube. *Development, 138*(22), 4921-4930. https://doi.org/10.1242/dev.070805

Vilardaga, J. P., Jean-Alphonse, F. G., & Gardella, T. J. (2014, Sep). Endosomal generation of cAMP in GPCR signaling. *Nat Chem Biol, 10*(9), 700-706. https://doi.org/10.1038/nchembio.1611

Walker-Gray, R., Stengel, F., & Gold, M. G. (2017, Sep 26). Mechanisms for restraining cAMP-dependent protein kinase revealed by subunit quantitation and cross-linking approaches. *Proc Natl Acad Sci U S A, 114*(39), 10414-10419. https://doi.org/10.1073/pnas.1701782114

Walsh, D. A., & Cooper, R. H. (1979). CHAPTER 1 - The Physiological Regulation and Function of cAMP-Dependent Protein Kinases. In G. Litwack (Ed.), *Biochemical Actions of Hormones* (pp. 1-75). Academic Press. https://doi.org/https://doi.org/10.1016/B978-0-12-452806-2.50007-8

Wang, B., Fallon, J. F., & Beachy, P. A. (2000, Feb 18). Hedgehog-regulated processing of Gli3 produces an anterior/posterior repressor gradient in the developing vertebrate limb. *Cell, 100*(4), 423-434. https://doi.org/S0092-8674(00)80678-9 [pii]

Wang, C., Pan, Y., & Wang, B. (2010, Jun). Suppressor of fused and Spop regulate the stability, processing and function of Gli2 and Gli3 full-length activators but not their repressors. *Development, 137*(12), 2001-2009. https://doi.org/dev.052126 [pii] 10.1242/dev.052126

Wang, L., & Dynlacht, B. D. (2018, Sep 17). The regulation of cilium assembly and disassembly in development and disease. *Development, 145*(18). https://doi.org/10.1242/dev.151407

Wen, X., Lai, C. K., Evangelista, M., Hongo, J. A., de Sauvage, F. J., & Scales, S. J. (2010, Apr). Kinetics of hedgehog-dependent full-length Gli3 accumulation in primary cilia and subsequent degradation. *Mol Cell Biol, 30*(8), 1910-1922. https://doi.org/10.1128/MCB.01089-09

Wolff, C., Roy, S., & Ingham, P. W. (2003, Jul 15). Multiple muscle cell identities induced by distinct levels and timing of hedgehog activity in the zebrafish embryo. *Curr Biol, 13*(14), 1169-1181. https://doi.org/10.1016/s0960-9822(03)00461-5

Ybot-Gonzalez, P., Cogram, P., Gerrelli, D., & Copp, A. J. (2002, May). Sonic hedgehog and the molecular regulation of mouse neural tube closure. *Development, 129*(10), 2507-2517. https://www.ncbi.nlm.nih.gov/pubmed/11973281

Ybot-Gonzalez, P., Gaston-Massuet, C., Girdler, G., Klingensmith, J., Arkell, R., Greene, N. D., & Copp, A. J. (2007, Sep). Neural plate morphogenesis during mouse neurulation is regulated by antagonism of Bmp signalling. *Development, 134*(17), 3203-3211. https://doi.org/10.1242/dev.008177

Ye, F., Nager, A. R., & Nachury, M. V. (2018, May 7). BBSome trains remove activated GPCRs from cilia by enabling passage through the transition zone. *J Cell Biol, 217*(5), 1847-1868. https://doi.org/10.1083/jcb.201709041

Yu, W., Wang, Y., McDonnell, K., Stephen, D., & Bai, C. B. (2009, Oct 1). Patterning of ventral telencephalon requires positive function of Gli transcription factors. *Dev Biol, 334*(1), 264-275. https://doi.org/10.1016/j.ydbio.2009.07.026

Zeidler, M. G., Van Keuren, M. L., & Saunders, T. L. (2011). BAC Transgenes, DNA Purification, and Transgenic Mouse Production. In S. Pease & T. L. Saunders (Eds.), *Advanced Protocols for Animal Transgenesis: An ISTT Manual* (pp. 159-179). Springer Berlin Heidelberg. https://doi.org/10.1007/978-3-642-20792-1_9

Zhang, J. Z., Lu, T. W., Stolerman, L. M., Tenner, B., Yang, J. R., Zhang, J. F., Falcke, M., Rangamani, P., Taylor, S. S., Mehta, S., & Zhang, J. (2020, Sep 17). Phase Separation of a PKA Regulatory Subunit Controls cAMP Compartmentation and Oncogenic Signaling. *Cell, 182*(6), 1531-1544 e1515. https://doi.org/10.1016/j.cell.2020.07.043

Zhao, T., Gan, Q., Stokes, A., Lassiter, R. N., Wang, Y., Chan, J., Han, J. X., Pleasure, D. E., Epstein, J. A., & Zhou, C. J. (2014, Jan). beta-catenin regulates Pax3 and Cdx2 for caudal neural tube closure and elongation. *Development, 141*(1), 148-157. https://doi.org/10.1242/dev.101550

Table 1. Results of breeding animals having *Gpr161 ko* and/or *mut1* alleles.

Breeding between *Gpr161 ko*/+ parents

Age	Litters	*wt/wt*	*ko/wt*	*ko/ko*
E8.5	16	36 (29%)	54 (44%)	33 (27%)
E9.5	26	51 (27%)	85 (45%)	54 (28%)
E10.25	8	16 (28%)	27 (47%)	15 (26%)
E10.5	6	14 (32%)	30 (68%)	0 (0%) **

Breeding *Gpr161 ko*/+ with *Gpr161 mut1*/+ parents

Age	Litters	*wt/wt*	*ko/wt* or *mut1/wt*	*mut1/ko*
E9.5	12	24 (26%)	45 (49%)	22 (24%)
E10.25	9	20 (31%)	28 (44%)	16 (25%)
E10.5	2	3 (21%)	7 (50%)	4 (29%)
E11.5	2	3 (21%)	7 (50%)	4 (29%)
E12.5	5	14 (35%)	23 (58%)	3 (7%)[1]
E13.5	4	8 (36%)	14 (64%)	0 (0%)[2, *]

Breeding between *Gpr161 mut1*/+ parents

Age	Litters	*wt/wt*	*mut1/wt*	*mut1/mut1*
E9.5	20	41 (30%)	61 (45%)	34 (25%)
E10.25	4	8 (25%)	16 (50%)	8 (25%)
E10.5	8	21 (30%)	34 (49%)	15 (21%)
E11.5	2	6 (43%)	4 (29%)	4 (29%)
E12.5	7	16 (29%)	27 (49%)	12 (22%)
E13.5	9	16 (27%)	29 (48%)	15 (25%)
E14.5	7	13 (30%)	23 (52%)	8 (18%)[3]
E14.75	6	13 (35%)	24 (65%)	0 (0%)[4, **]
E15.5	5	10 (38%)	16 (62%)	0 (0%)[5, ***]

[1] 3 dead *mut1/ko* embryos were not counted
[2] 7 dead *mut1/ko* embryos were not counted
[3] 7 dead *mut1/mut1* embryos were not counted
[4] 13 dead *mut1/mut1*embryos were not counted
[5] Dead or resorbed embryos were not counted

* $p<0.05$ by Chi Square test
** $p<0.01$ by Chi Square test
*** $p<0.001$ by Chi Square test

1

Table 2. Phenotypes in *Gpr161* mutants.

Phenotype (Analysis age)	*Gpr161*$^{ko/ko}$	*Gpr161*$^{ko/mut1}$	*Gpr161*$^{mut1/mut1}$
Lethality of embryos	E10.5	E13.5	E14.75
Exencephaly (>E10.25)	100% (102/102)	100% (54/54)	100% (12/12)
Spina bifida (>E10.25)	100% (15/15)	100% (16/16)	N/D
Midface widening (>E12.5)	N/A	N/A	100% (23/23)
Microphthalmia (>E12.5)	N/A	100% (3/3)	100% (35/35)
Pericardial effusion (E12.5-13.5)	N/A	92% (11/12)	N/D
Limb development			
Forelimb	No forelimbs at E10.25	Stunted at E12.5	Polydactyly at E13.5 (6~7 digits)
Hindlimb	Present	Present	Polydactyly at E13.5 (6~7 digits)
Kinked tail (> E12.5)	N/A	100% (3/3)	N/D

N/A, not applicable, N/D, not determined.

Figure legends

Figure 1. A ciliary localization defective *Gpr161* mutant is competent for cAMP signaling.

(A) Cartoon representing the VKARK>AAAAA mut1 mutation in the third intracellular loop of mouse Gpr161.

(B) Confluent NIH 3T3 Flp-In CRISPR-based *Gpr161* knockout (ko) cells stably expressing untagged wildtype (wt) or Gpr161^{mut1} were starved for 24h, fixed, and immunostained with anti-Gpr161 (green), anti-acetylated tubulin (AcTub; red) antibodies and counterstained for DNA (blue). Arrowheads indicate cilia.

(C) – (D) RPE hTERT cells stably expressing C-terminal LAP-tagged *Gpr161^{wt}* or *Gpr161^{mut1}* constructs were sequentially transfected with control or *INPP5E* siRNA (100 nM) twice and cultured for a total of 72 h. The cells were serum starved for the last 24 h before fixation and immunostained with anti-GFP (green), anti-TULP3 (red), anti-acetylated tubulin (AcTub; magenta) antibodies and counterstained for DNA (blue). GPR161 and TULP3 positive cells were quantified. Arrowheads in (D) indicate cilia. Total 6-12 different images quantified from 2 experiments, and total 600-2000 cells counted/condition. Data shown as mean ± SD. ****, p<0.0001. Other pairwise comparisons are not significantly different.

(E) – (F) Quantification of LAP-tagged Gpr161 (E) and TULP3 (F) pixel intensities from C shown as violin plots. Total counted cells were >60/condition. A.U., arbitrary units. ****, p<0.0001; ***, p p<0.001.

(G) Doxycycline-inducible NIH 3T3 Tet-on 3G cells expressing untagged *Gpr161^{wt}* or *Gpr161^{mut1}* were induced for 24h with 2μg/ml doxycycline. The cells were subjected to TR-FRET cell-based assays for assaying cAMP. cAMP levels (nM) were calculated as interpolated values from a standard curve. Data from triplicate wells (mean ± SD) and is representative of 3 independent experiments. Mean *Gpr161* transcript levels are shown below. **, p<0.01. ns, not significant.

Scale: (B) and (D), 10 μm.

Figure 1-figure supplement 1. Gpr161^{mut1} was not accumulated in cilia of β–arrestin 1/2 double knockout MEFs. Wild type or β–arrestin 1/2 double knockout (*Arrb1/Arrb2* dko) MEFs stably expressing LAP-tagged Gpr161^{wt} or Gpr161^{mut1} were starved for 24 h followed by SAG (500 nM) treatment for further 24 h. Cells were fixed and immunostained with anti-GFP (green), anti-Gpr161 (red), anti-acetylated tubulin (AcTub; magenta) antibodies and counterstained for DNA (blue). Quantification below (mean ± SD) shows that Gpr161^{mut1}was not accumulated in cilia of *Arrb1/Arrb2* dko MEFs irrespective of Hh pathway activation by SAG, despite accumulation of endogenous Gpr161 in the same cells. Arrows depict cilia. Scale, 10 μm.

Figure 1-figure supplement 2. Gpr161^{mut1} was not accumulated in cilia upon *BBS4* knockdown in RPE-hTERT cells. RPE-hTERT cells stably expressing LAP-tagged Gpr161^{wt} or Gpr161^{mut1} were treated with 100 nM siRNA against *BBS4* for 48 h before starving for 24 h. Fixed cells were immunostained with anti-GFP (green), anti-Gpr161 (red), anti-acetylated tubulin (AcTub; magenta) antibodies and counterstained for DNA (blue). Violin plot of ciliary intensities shows that LAP-tagged Gpr161^{wt} accumulated in cilia upon *BBS4* knockdown in RPE-hTERT cells, but LAP-tagged Gpr161^{mut1} did not accumulate unlike accumulation of endogenous Gpr161 in the same cells. Arrows depict cilia. ****, p<0.0001; ***, p<0.001; ns, not significant. Scale bar, 10 μm.

Figure 1-figure supplement 3. Gpr161^{mut1} containing vesicles co-label with endocytosed transferrin similar to Gpr161^{wt}. Wild type MEFs stably expressing LAP-tagged Gpr161^{wt} or Gpr161^{mut1} were starved for 48 h followed by treatment with Transferrin conjugated with Alexa Fluor 568 (Tf568) or 30 min at 37ºC. Fixed cells were immunostained with anti-GFP (green), anti-acetylated tubulin and γ-tubulin (AcTub; γTub magenta) antibodies and counterstained for DNA. We previously demonstrated that Gpr161 containing vesicles to be recycling endosomes that co-label with endocytosed transferrin (Mukhopadhyay et al., 2013). Arrows point to cilia. Similar to LAP-tagged Gpr161^{wt}, LAP-tagged Gpr161^{mut1} containing vesicles co-labeled with endocytosed transferrin. Scale bar, 10 μm.

Figure 2. Generating ciliary localization defective endogenous knock-in *Gpr161^{mut1}* mouse model.

(A) The gene targeting strategy used to engineer the *Gpr161^{mut1}* allele. Exons are numbered based on NM_001081126.2. PGKneo and FRT cassettes and genotyping (GT) primer sequences are indicated. The *mut1* sequence is located on Exon 4.
(B) Southern blot analysis of representative ES cell clones using the 5' and 3' probes in A.
(C) Sanger sequencing of *Gpr161^{wt}* and *Gpr161^{mut1}* alleles in adult mouse-tail DNA. Double peaks in *Gpr161$^{wt/mut1}$* heterozygote indicated by arrowheads. The engineered NotI restriction site (GCGGCCGC) is indicated by a purple bar.
(D) Genotyping for wild type, *Gpr161^{mut1}* and knockout (ko) alleles by PCR using designated primers shown in A and digesting with NotI.
(E) qRT-PCR of *Gpr161* transcripts normalized to *Hprt* in whole embryo extracts at E9.5 indicate diminished mRNA expression in the *Gpr161* knockout (*ko/ko*) embryos compared to wild type (*wt/wt*), but unchanged in *mut1/mut1* embryos. Data shown as mean ± SD. n=3 (*wt/wt*), 5 (*ko/wt*), 4 (*mut1/wt*), 3 (*ko/ko*), 3 (*ko/mut1*), 2 (*mut1/mut1*) embryos. *, $p<0.05$; ***, $p<0.001$. Other pairwise comparisons are not significantly different.

Figure 2- figure supplement 1.
(A) Genomic DNA sequence of *Gpr161mut1* allele, after deletion of the FRT-PGKneo-FRT cassette by crossing with Flp-O mice.
(B) Scheme for generating *mut1* allele. Details in Methods.

Figure 2-figure supplement 2. Tandem affinity purification of LAP-tagged Gpr161^{wt} or Gpr161^{mut1} (see Methods) stably expressed in wild type MEFs was followed by immunoblotting for S-tag. Inputs show lysates before tandem affinity purification that were immunoblotted for α-tubulin.

Figure 2-figure supplement 3. The ciliary morphologies (A), including ciliary lengths (B) in *Gpr161$^{ko/mut1}$* embryos at ~E10.25 in mesenchyme (MES), somatopleuric mesoderm (SP) or in the neural tube (NT) were unaffected compared to control wild type (*wt*) embryos. Thorcaic level sections were counterstained with Arl13b (red) and DAPI (blue). Scale, 10 µm. Data shown as mean ± SD. Total counted cilia were >30.

Figure 3. *Gpr161^{mut1}* allele is hypomorphic to knockout.

(A) – (F) Bright-field images of wild type (*wt/wt*), *Gpr161* knockout (*ko/ko*), *mut1/ko* heterozygote, and *mut1* homozygote (*mut1/mut1*) at indicated time points. Red arrowhead indicates no limb bud in knockout embryo. *En face* view of E10.5 and E13.5 embryos in (E). Black dotted line or asterisk, rostral malformation; yellow arrow and dotted line, spina bifida; red dotted line, forelimb; blue dotted line, hindlimb. See also Tables 1 and 2.

Scale: (A), 1 mm; (B-D), 2 mm; (D); (E), 1 mm.

Figure 4. *Gpr161*$^{mut1/ko}$ embryos have reduced Hh pathway hyperactivation compared to knockouts.

(A) – (B) *Gli1* (A) and *Ptch2* (B) transcript levels in whole-embryo extracts at E9.5 qRT-PCR, normalized to *Gapdh*, n = 3-4 embryos each, data shown as mean ± SEM. **, p<0.01, ***, p<0.001, ****, p<0.0001. Only significant differences are marked.

(C) Immunoblotting for Gli1, Gli3 and α-tubulin in whole-embryo lysates at E9.5. n=2 or 3 independent experiments for Gli1 or Gli3 immunoblotting, respectively. Data shown as mean ± SD normalized to α-tubulin. *, p<0.05; **, p<0.01; ***, p<0.001; ****, p<0.0001.

(D) NIH 3T3 Flp-In CRISPR based *Gpr161* ko cells stably expressing untagged wildtype (*wt*) or *Gpr161*^{mut1} were starved for 24 h upon confluence and were treated for further 24 h ± SAG (500 nM). After fixation, cells were immunostained with anti-Gli2 (red), anti-Gpr161 (green), anti-acetylated and γ-tubulin (AcTub; γTub grey) antibodies.

(E) Quantification of Gli2 positive cilia from (D). n=100 cells counted/condition from two coverslips each. Data shown as mean ± SD. **, p<0.01.

Scale: (E), 5 μm.

Figure 4-figure supplement 1. Immunoblotting for Gli2 and α-tubulin in E9.5 whole-embryo lysates. n = 2. Data shown as mean ± SD.

Figure 5. *Gpr161$^{mut1/ko}$* embryos exhibit less ventralized neural tube compared to *Gpr161* knockouts.

Topmost panels show bright-field images of wildtype (*wt*)*, Gpr161 ko, Gpr161 mut1/ko, Gpr161 mut1/mut1, Gpr161; Gli2* double *ko*, and *Gli2 ko* whole-mount embryos at E9.5. Bottom panels show rostral neural tube horizontal sections immunostained using designated markers. All images are counterstained with Hoechst. Black dotted line mark rostral malformations. Vertical bars show the extent of dorsoventral expression of markers. Asterix, nonspecific background staining outside neural tube. n=2 to 4 embryos each genotype and immunostaining.
Scale: 50 µm.

Figure 5- figure supplement 1. *Gpr161$^{mut1/ko}$* embryos exhibit less ventralized neural tube compared to *Gpr161* knockouts. Quantification of dorsoventral (D-V) extent of Nkx6.1 expression to that of the neural tube (**Figure 5**) shows similar levels of partial ventralization in *Gpr161 mut1/ko* and *Gpr161; Gli2* double *ko* compared to *Gpr161 ko/ko* and normal extent of expression in *Gpr161 mut1/mut1.* Quantification (mean ± SEM) at thoracic region from 2-4 embryos (each shown by a different shape). For each embryo, average from 2 or more sections were taken. ****, $p<0.0001$.

Figure 6. *Gpr161*$^{mut1/mut1}$ embryos exhibit high Hh signaling and polydactyly in limb buds.

(A) – (C) RNA *in situ* hybridization for E10.5 *Ptch1* (A), *Shh* (B) *Hoxd13* (C) limb buds. Control (*Gpr161*$^{mut1/wt}$) in (A-B). *Ptch1* and *Hoxd13* were expanded anteriorly in *Gpr161*$^{mut1/mut1}$ limb buds. Shh was diffusely expressed posteriorly but was not ectopically expressed anteriorly in *Gpr161*$^{mut1/mut1}$ limb buds. n=2-5 each.

(D) Immunoblotting of forelimb (FL) and hindlimb (HL) buds for Gli3 and α-tubulin shows decreased Gli3R levels at E12.5 wildtype (wt) versus *Gpr161*$^{mut1/mut1}$. Quantification shown is normalized to α-tubulin. n = 3 experiments. *, $p<0.05$; **, $p<0.01$.

(E) RNA *in situ* hybridization for *Sox9* and *Col2a1* in E13.5 wildtype and *Gpr161*$^{mut1/mut1}$ limb buds. *Gpr161*$^{mut1/mut1}$ limb buds show polydactyly. n=4 each.

Scale: (A-C), 50 μm; (E), 500 μm. Also see source data for Figure 6D.

Figure 7. *Gpr161*$^{mut1/mut1}$ embryos show high Hh signaling and mid face widening.

(A) RNA *in situ* hybridization for *Ptch1* in wildtype (*wt*), *Gpr161*$^{mut1/mut1}$, and *Wnt1-Cre*; *Gpr161*$^{f/f}$ E12.5 head. Distances between nasal pits are shown as bidirectional arrows. Lateral and frontal views are shown. n=3-4 each

(B) RNA *in situ* hybridization for *Ptch1* in E13.5 wildtype (*wt*), *Gpr161*$^{mut1/mut1}$ head. Top panels, lateral view; middle panels, frontal tilted view shows palate and tongue; bottom panels, sagittal section showing tongue. Black dotted lines in the bottom panels indicate tongue. Bidirectional arrows show increased distance between nasal pits. Arrow points to prominent palatal shelf in *Gpr161*$^{mut1/mut1}$. n=3 each

(C) RNA *in situ* hybridization for *Gli1* in E12.5 wildtype (*wt*), *Gpr161*$^{mut1/mut1}$ head. Top panels, frontal view. Middle panels show palates imaged from below (palatal view) and bottom panels show lower jaw viewed from above (tongue view) after separating the jaws. Arrows in upper panel show secondary palatal shelves. Black dotted lines in the bottom panels indicate tongue. Note increased gap between maxillary processes by ingression of median nasal processes. n=3 each

(D) – (E) Quantification of distance between nasal pits as shown in (A). The colors are matched with each strain in A and B. Error bars represent SEM. ***, $P<0.001$; ****, $P<0.0001$, unpaired t-test. n=3-4 each.

(F) RNA *in situ* hybridization for *Ptch1* in E12.5 control (*Gli2*$^{-/+}$), *Gpr161; Gli2* double ko and *Gli2* ko head. Note persistent exencephaly in *Gpr161; Gli2* double ko and midfacial widening. Displaced lower jaw is an artifact (*). n=1-2 each

Scale: (A) and (F), 1 mm; (B) and (C) 2 mm.

Abbreviations: ex, exencephaly; mnp, medial nasal process; mx, maxillary process; mn, mandibular process; np, nasal pit; ps, palatal shelf; t, tongue.

Figure 8. Gpr161 ciliary pools determine Hh pathway repression-regulated morpho-phenotypic spectrum.

(A) Neural tube development. Hh is expressed from the notochord (blue). Gli2A-mediated threshold activation mediates floorplate and ventral-most progenitor patterning. Gli3R regulates intermediate level patterning. Lack of cilia prevents patterning of all ventral progenitors. Complete lack of Gpr161 in ko causes ventralization of all ventral progenitors from excessive Gli2A generation and loss of Gli3R. Lack of Gpr161 ciliary pools in *Gpr161*$^{mut1/ko}$ reduces Gli3R formation sufficiently to cause intermediate level expansion of Nkx6.1 but does not generate excessive GliA to cause ventralization of floor plate markers. Caudal spina bifida and exencephaly persists in *Gpr161*$^{mut1/ko}$ embryos similar to *Gpr161* ko.

(B) Limb development. Before Shh expression, Gli3R gradient is set up by posterior dHand gradient that is established in posterior mesenchyme. Shh expression from ZPA starting from E9.75 establishes posterior gradient of pathway targets such as *Ptch1/Gli1*. Anterior Gli3R gradient also regulates expression of genes in posterior mesenchyme such as *Hoxd13*. Lack of cilia causes preaxial polydactyly from increased *5'Hoxd* gene expression arising from lack of Gli3R. *Gpr161* ko prevents forelimb formation. Conditional deletion of *Gpr161* in limb mesenchyme using *Prx1-Cre*; *Gpr161*$^{f/f}$ (*Prx1-Gpr161 c*ko) causes increased Hh pathway targets, expanded *Hoxd13* and lack of Gli3R in limb buds contributing to polydactyly. Lack of Gpr161 ciliary pools in *Gpr161*$^{mut1/mut1}$ shows increased Hh pathway targets, expanded *Hoxd13* and lack of Gli3R in limb buds contributing to polydactyly. The Shh expression in the posterior limb bud is diffuse, likely from lack of counter-antagonism between Gli3R and dHand. Abbreviations: AER, anterior ectodermal ridge; ZPA, zone of polarizing activity; A, anterior; P, posterior, Pr, proximal; D, distal.

(C) Facial development. Shh is expressed from the frontonasal ectodermal zone in the medial nasal processes. Threshold repression by both Gli2R and Gli3R prevents midfacial widening. Lack of cilia, or lack of both Gli2/3 causes midfacial widening, which is prevented by forced Gli3R expression. Lack of Gpr161 ciliary pools in *Gpr161*$^{mut1/mut1}$ phenocopies *Gpr161* deletion in craniofacial mesenchyme using *Wnt1-Cre*; *Gpr161*$^{f/f}$ (*Wnt1-Gpr161 c*ko) in showing midfacial widening and increased levels of Shh pathway targets. Gli2 loss is unable to rescue midfacial widening and increased Shh pathway targets in *Gpr161* ko background, suggesting lack of GliR contributing to these phenotypes. Abbreviations: FEZ, frontonasal ectodermal zone; LNP, lateral nasal process; MNP, medial nasal process, Mx, maxillary process.

(D) Model of Gpr161 ciliary and extraciliary pools in Hh pathway. Both ciliary and extraciliary pools of Gpr161 contribute to GliR formation by PKA-mediated phosphorylation. Complete lack of Gpr161 prevents Gli2/3 phosphorylation by PKA. Gli2 is less efficient in repressor formation than Gli3. Unphosphorylated Gli2 is dissociated from Sufu and accumulates in ciliary tips. GliA formation is dependent on lack of PKA phosphorylation but likely occurs downstream of Gli2 accumulation in ciliary tips. Smo might further promote GliA formation. Gli2 accumulation in ciliary tips and GliA formation also occurs in *Ankmy2* knockout where trafficking of ACs to cilia is affected. Lack of ciliary Gpr161 prevents ciliary cAMP mediated PKA activation but does not hinder extraciliary Gpr161 from cAMP production. Such extraciliary production might happen in the endomembrane compartment, but mechanisms of PKA activation and PKA regulatory subunits involved are not known. Such restricted phosphorylation limits Gli3R formation but is still sufficient to dissociate Gli2 from Sufu causing accumulation in ciliary tips. However, GliA formation is impacted. Tissue regions that depend on GliR are specifically affected from loss of ciliary pools of Gpr161. Abbreviations: RI/RII, type I and type II PKA regulatory subunits.

1 # Appendix

2

Key Resources Table				
Reagent type (species) or resource	**Designation**	**Source or reference**	**Identifiers**	**Additional information**
genetic reagent (*M. musculus*)	*Gpr161*$^{mut1/+}$	This study		See Methods
genetic reagent (*M. musculus*)	*Gpr161*$^{ko/+}$	Hwang et al., 2018	RRID:MGI:6357708	
genetic reagent (*M. musculus*)	*Gpr161*$^{f/f}$	Hwang et al., 2018	RRID:MGI:6357710	
genetic reagent (*M. musculus*)	*Wnt1-Cre*	Jackson Laboratory	Jax strain No: 022501	Lewis et al., 2013
genetic reagent (*M. musculus*)	*Prx1-Cre*	Jackson Laboratory	Jax strain No: 005584	Logan et al., 2002
genetic reagent (*M. musculus*)	*Gli2*^{tm1Alj}	Mo et al. 1997	RRID:MGI:1857509	
cell line (*Homo sapiens*)	RPE hTERT	ATCC	ATCC CRL-4000; RRID:CVCL_4388	
cell line (*M. musculus*)	NIH 3T3 Tet-on 3G	Clontech	631197; RRID:CVCL_V360	
cell line (*M. musculus*)	NIH-3T3 Flp-In	Thermo Fisher Scientific	R76107	
cell line (*M. musculus*)	*Gpr161* ko NIH-3T3 Flp-In	Pusapati et al., 2018		Gift from Rajat Rohatgi
cell line (*M. musculus*)	β-arrestin 1/2 double knockout MEFs	Kovacs et al., 2008		Gift from R. Lefkowitz

transfected construct (*Homo sapiens*)	INPP5E On-target plus siRNA	Dharmacon/ Horizon, Perkin Elmer	Humbert et al., 2012 J-020852-05	5′-GGAAUUAAAAGACGGAUUU-3’
transfected construct (*Homo sapiens*)	BBS4 siGenome siRNA	Dharmacon/ Horizon, Perkin Elmer	Loktev et al., 2008 D-013649-04	5′-CGAUCUGACUUAUAUAAUG-3’
antibody	Mouse monoclonal anti-Acetylated tubulin	Sigma	Cat# T6793 RRID: AB_477585	IF (1:5000)
antibody	Mouse monoclonal anti-Arl13b	NeuroMab Facility	Cat# N295B/66 RRID: AB_2750771	IF (1:500)
antibody	Mouse monoclonal anti-ɣ-tubulin	Sigma	Cat# T6557 RRID: AB_532292	IF (1:500)
antibody	Mouse monoclonal anti-α-tubulin	Sigma	Cat# T6199 RRID: AB_477583	WB (1:5000)
antibody	Rabbit polyclonal anti-FoxA2	Abcam	Cat# ab40874 RRID: AB_732411 or Cat# ab108422 RRID: AB_11157157	IF (1:2000)
antibody	Mouse monoclonal anti-Nkx6.1	DSHB	Cat# F55A10-s RRID: AB_532378	IF (1:500)
antibody	Rabbit polyclonal anti-Pax6	Biolegend	Cat# 901302 RRID: AB_2749901	IF (1:50)
antibody	Mouse monoclonal anti-Pax7	DSHB	RRID: AB_528428	IF (1:50)

antibody	Guinea pig anti-Gli2	Gift from Jonathan Eggenschwiler	Cho et al, 2008	IF (1:500)
antibody	Chicken anti-GFP	Abcam	Cat# ab13970 RRID: AB_300798	IF (1:10000)
antibody	Rabbit polyclonal anti-Gpr161	Custom-made	Pal et al, 2016	IF (1:250)
antibody	Rabbit polyclonal anti-Tulp3	Gift from Jonathan Eggenschwiler	Norman et al, 2009	IF (1:500)
antibody	Goat polyclonal anti-Gli3	R&D Systems	AF3690	WB (1:1000)
antibody	Goat polyclonal anti-Gli2	R&D Systems	AF3635	WB (1:1000)
antibody	Mouse monoclonal anti-Gli1	Cell Signaling RRID: AB_2294746	Cat# 2643	WB (1:1000)
antibody	Alexa Fluor 488-, 555-, 594-, 647-conjugated secondary antibodies	Life Technologies, Carlsbad, CA		IF (1:2000)
antibody	IRDye tagged secondary antibodies	LI-COR		IF (1:5000)
antibody	Hoechst 33342	Life Technologies		IF (1:5000)
recombinant DNA reagent	pgLAP5 vector (plasmid)	Addgene	Plasmid #19706; RRID: Addgene_19706	
recombinant DNA reagent	pDONR221_Gpr161 (*M. musculus*)	Mukhopadhyay et al., 2013	Synthesized by DNA2.0	NM_001081126.1
sequence-based reagent	*Gpr161 mut1* F	This paper	PCR primers	CAG AAA GCA ACA GCA AAG CA

sequence-based reagent	*Gpr161 mut1* R	This paper	PCR primers	ACC CTG ACA CTG CCC TTA GC
sequence-based reagent	*Gpr161* Ex4 F	Hwang et al., 2018	PCR primers	CAA GAT GGA TTC GCA GTA GCT TGG
sequence-based reagent	*Gpr161* floxed R	Hwang et al., 2018	PCR primers	ATG GGG TAC ACC ATT GGA TAC AGG
sequence-based reagent	*Gpr161 Neo cassette* R	Hwang et al., 2018	PCR primers	CAA CGG GTT CTT CTG TTA GTC C
sequence-based reagent	Cre-F	Hwang et al., 2018	PCR primers	AAT GCT GTC ACT TGG TCG TGG C
sequence-based reagent	Cre-R	Hwang et al., 2018	PCR primers	GAA AAT GCT TCT GTC CGT TTG C
sequence-based reagent	Gli2 sense	Mo et al., 1997	PCR primers	AAA CAA AGC TCC TGT ACA CG
sequence-based reagent	Gli2 antisense	Mo et al., 1997	PCR primers	CAC CCC AAA GCA TGT GTT TT
sequence-based reagent	pPNT	Mo et al., 1997	PCR primers	ATG CCT GCT CTT TAC TGA AG
sequence-based reagent	Gli1-F	Sigma	*Gli1* TaqMan probes for qRT-PCR	GCA GTG GGT AAC ATG AGT GTC T
sequence-based reagent	Gli1-R	Sigma	*Gli1* TaqMan probes for qRT-PCR	AGG CAC TAG AGT TGA GGA ATT GT
sequence-based reagent	Gli1-Probe (FAM/TAMRA)	Sigma	*Gli1* TaqMan probes for qRT-PCR	CTC TCC AGG CAG AGA CCC CAG C
sequence-based reagent	Ptch2-F	Sigma	*Ptch2* TaqMan probes for qRT-PCR	CAG AGT GAC TAC CTC CAT GAC TGT

sequence-based reagent	Ptch2-R	Sigma	*Ptch2* TaqMan probes for qRT-PCR	GCT GGG TGG ACG TAT GCT
sequence-based reagent	Ptch2-probe (FAM/TAMRA)	Sigma	*Ptch2* TaqMan probes for qRT-PCR	CTC CAC CCA CCA CCT CTG CCT
sequence-based reagent	Taqman probes for *Gpr161*	Applied Biosystems	Mm01291057_m1	
sequence-based reagent	Taqman probes for *Gapdh*	Applied Biosystems	Mm99999915	
commercial assay or kit	TR-FRET cAMP assay	Cisbio	62AM4PEB	
commercial assay or kit	GenElute mammalian total RNA purification kit	Sigma	RTN350	
commercial assay or kit	SYBR Green Quantitative RT-qPCR Kit	Sigma	QR0100	
commercial assay or kit	Mycoplasma PCR Detection Kit	Genlantis	MY01050	
commercial assay or kit	Kicqstart One-Step Probe RT-qPCR ReadyMix	Sigma	KCQS07	
chemical compound, drug	Penicillin/Streptomycin	Sigma	P4333	Cell culture
chemical compound, drug	Glutamine	Sigma	G7513	Cell culture
chemical compound, drug	Polyfect	Qiagen	301105	Cell culture

chemical compound, drug	DMEM-High Glucose	Sigma	D5796	Cell culture
chemical compound, drug	DMEM F12	Sigma	D6421	Cell culture
chemical compound, drug	BCS	Sigma	12133C	Cell culture
chemical compound, drug	FBS	Sigma	F0926	Cell culture
chemical compound, drug	Paraformaldehyde	Electron microscopy solutions	15710	
chemical compound, drug	Normal donkey serum	Jackson ImmunoResearch, West Grove, PA	Cat# 017-000-121; RRID:AB_2337258	
chemical compound, drug	Fluoromount-G	Southern Biotech	0100-01	
chemical compound, drug	Permount	ThermoFisher Scientific	SP15-100	
software, algorithm	ImageJ software		RRID:SCR_003070	
software, algorithm	GraphPad Prism		RRID:SCR_002798	

1

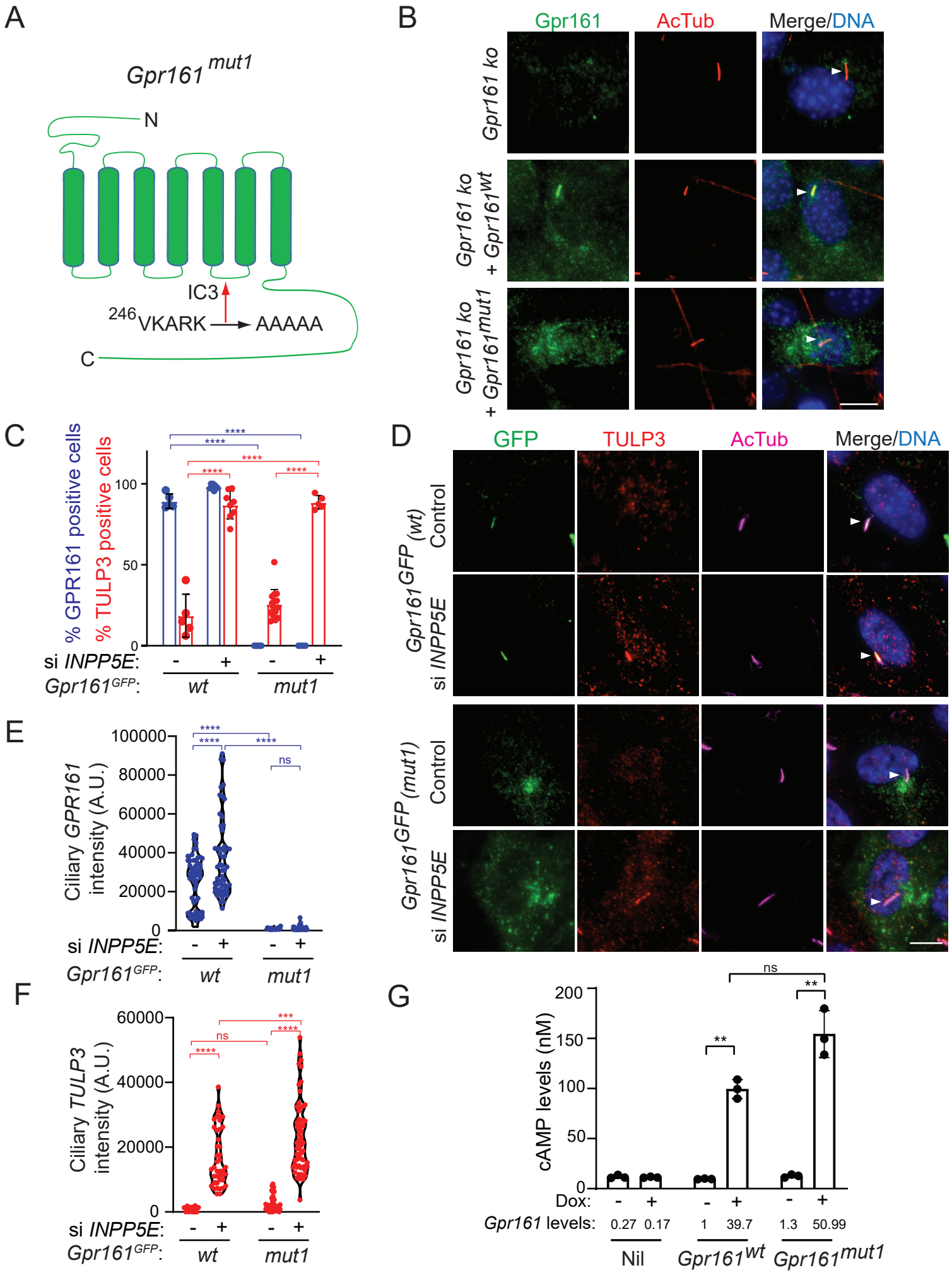
A
Gpr161 mut1
N
IC3
246VKARK
AAAAA
C
B
Gpr161
AcTub
Merge/DNA
Gpr161 ko
Gpr161 ko + Gpr161wt
Gpr161 ko + Gpr161mut1
C
% GPR161 positive cells
% TULP3 positive cells
si INPP5E:
Gpr161GFP:
wt
mut1
D
GFP
TULP3
AcTub
Merge/DNA
Gpr161GFP (wt)
Gpr161GFP (mut1)
Control
si INPP5E
E
Ciliary GPR161 intensity (A.U.)
ns
F
Ciliary TULP3 intensity (A.U.)
G
cAMP levels (nM)
Dox:
Gpr161 levels:
0.27 0.17
1 39.7
1.3 50.99
Nil
Gpr161wt
Gpr161mut1

Hwang_Figure 1- Supplement 1

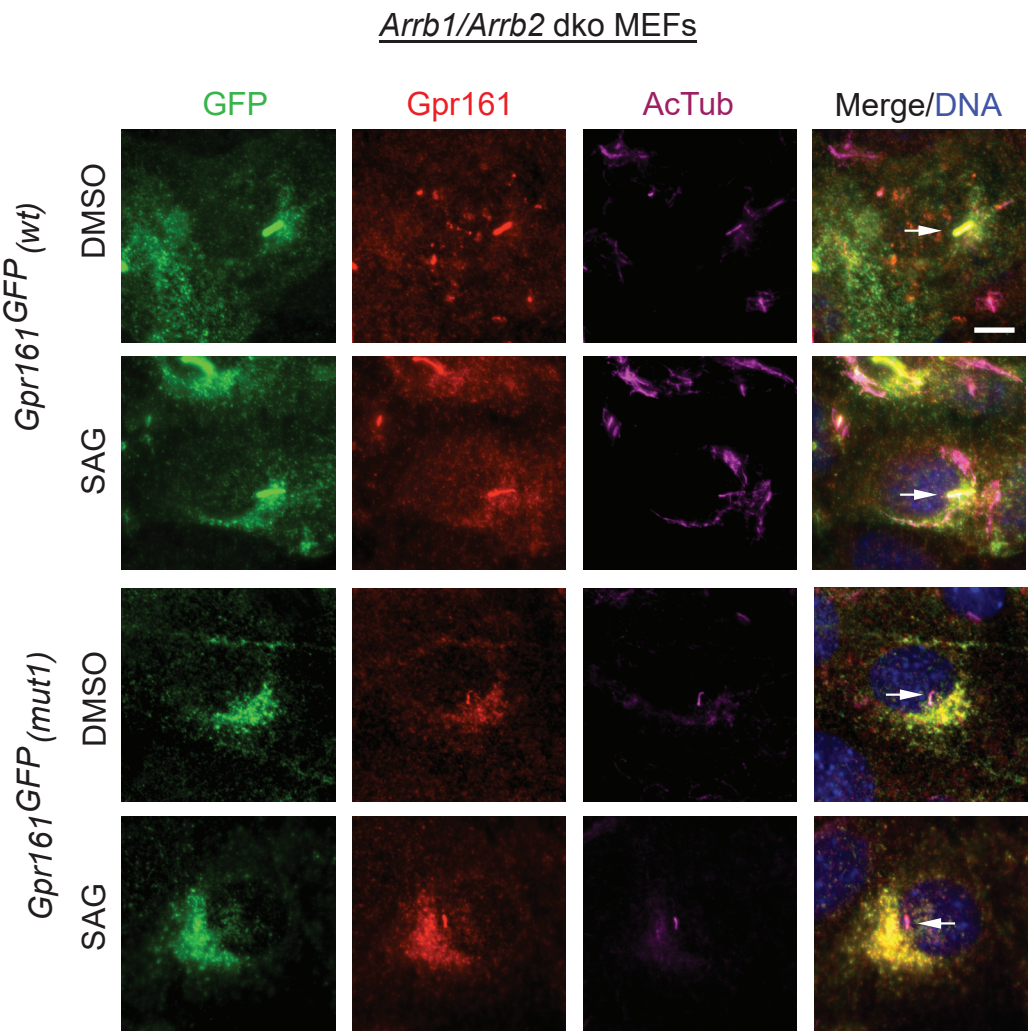

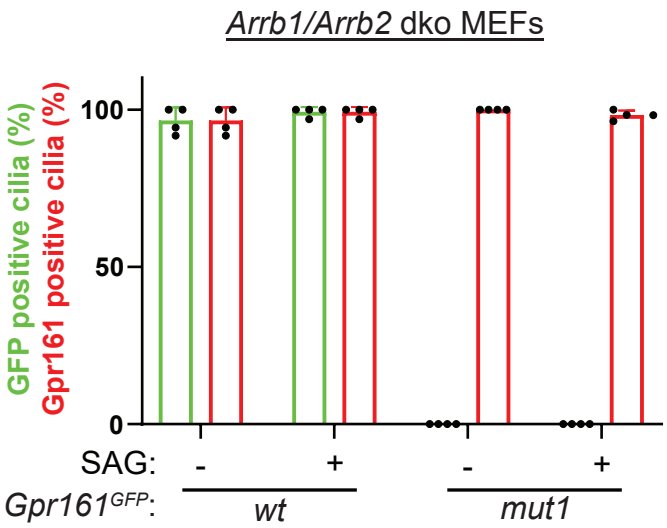

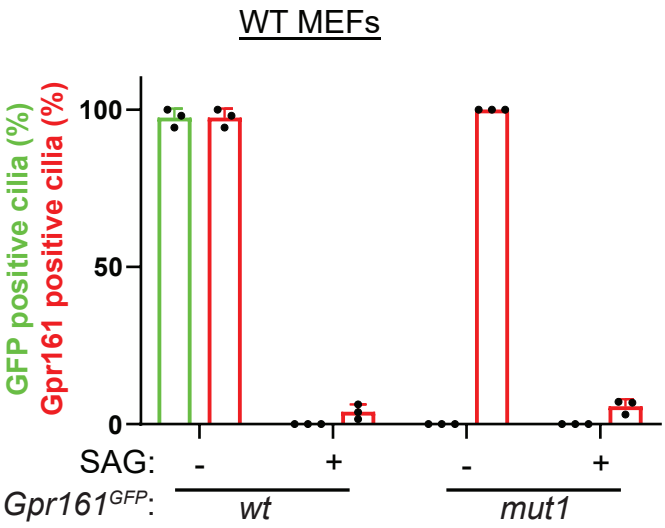

Hwang_Figure 1- Supplement 2

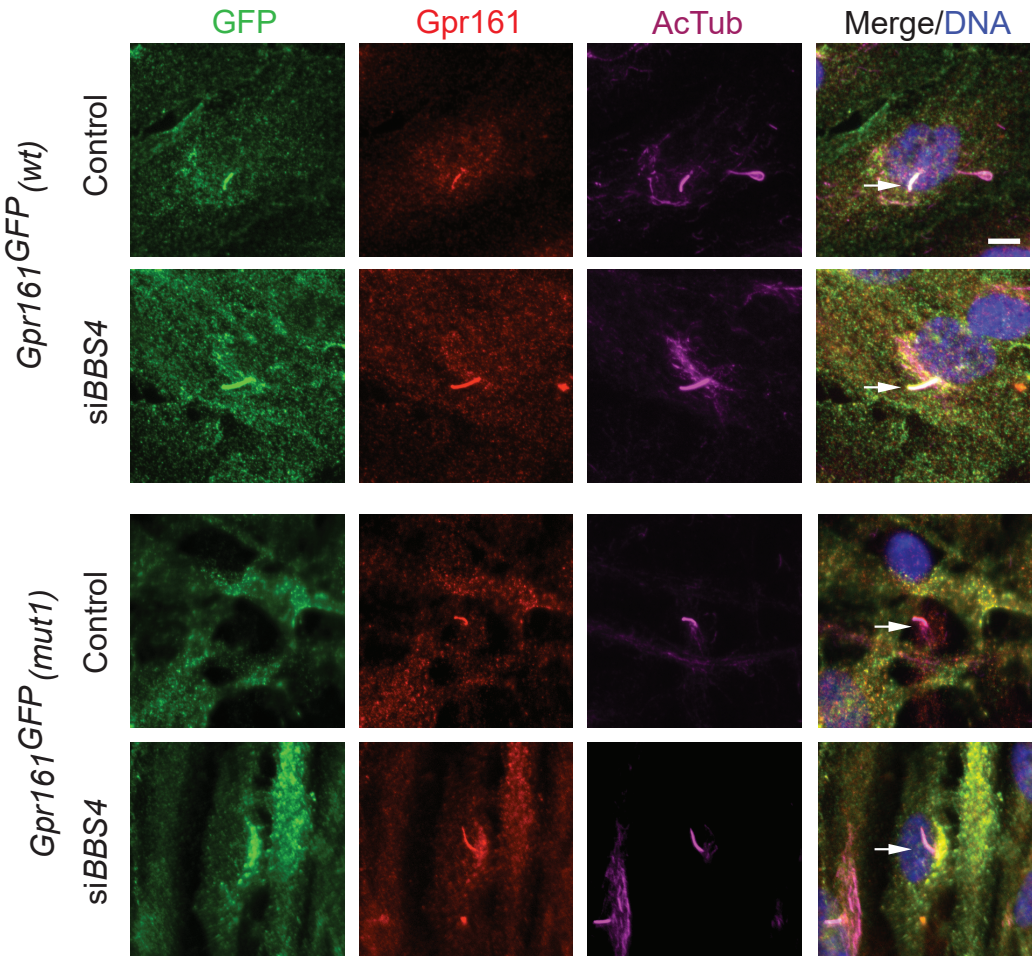

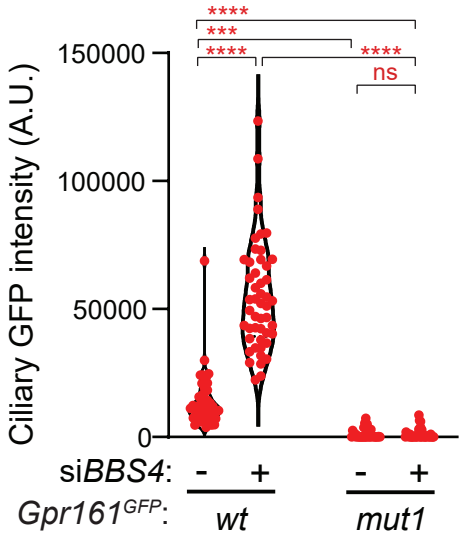

Hwang_Figure 1- Supplement 3

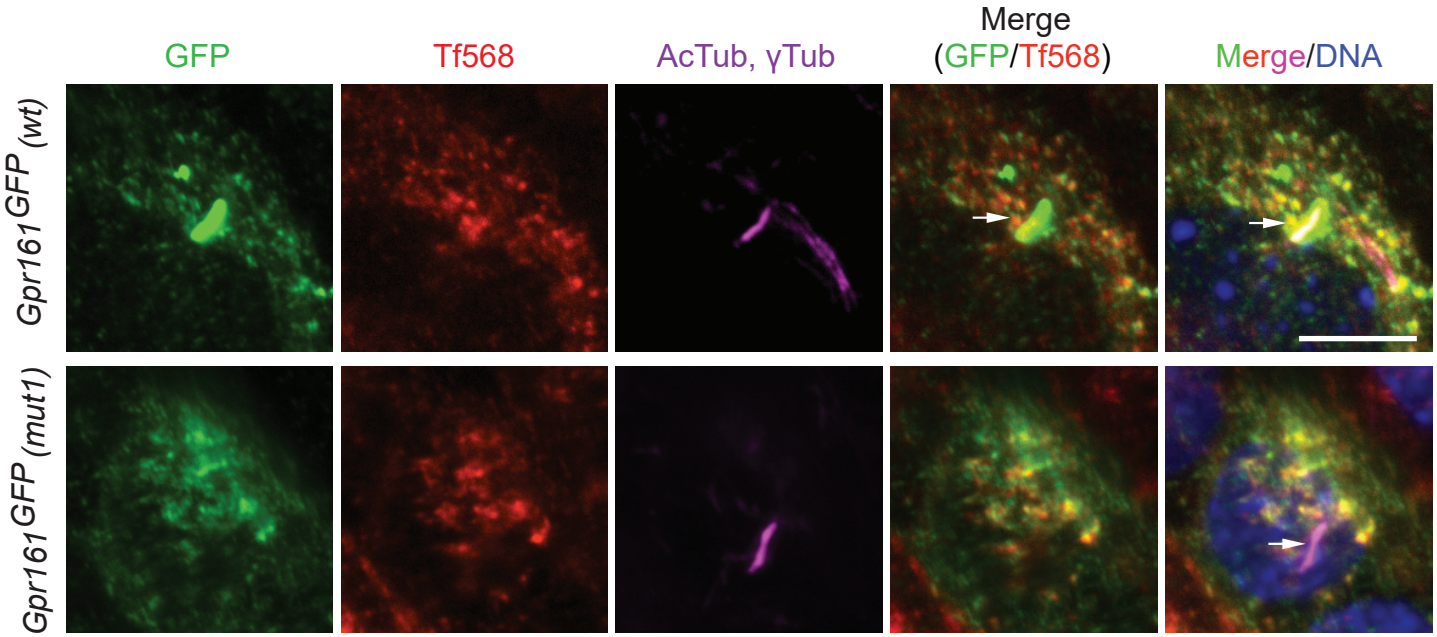

Hwang_Figure 2

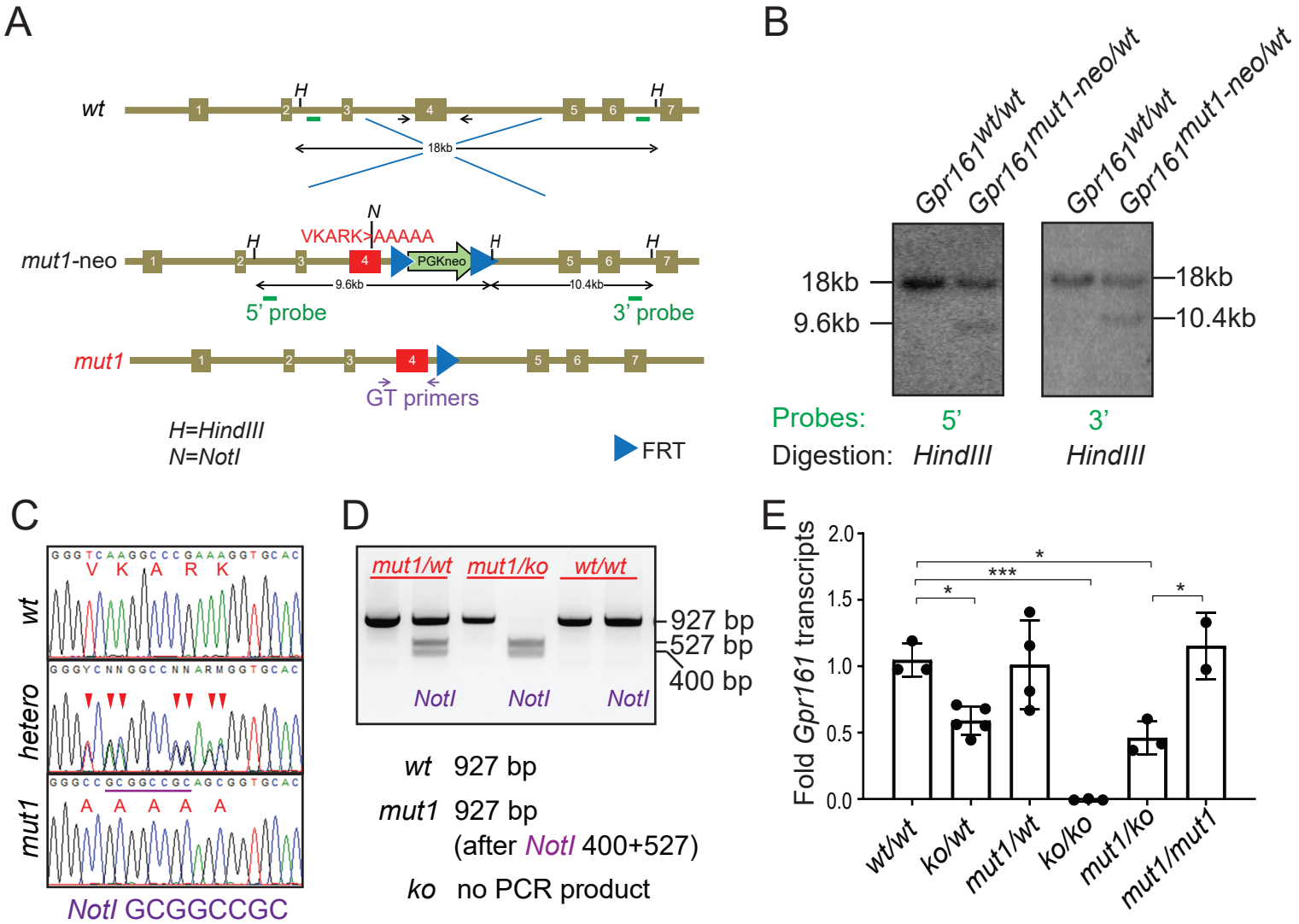

A

Gpr161 Exon 4 mutation

V K A R K → A A A A A

GTCAAGGCCCGAAAG → GcCgcGGCCgcAgcG

NotI

ctaaatgttttttaaaaggcaatacagaaagcaacagcaaagcaaatagaaagcagattaggataattcctctctcccctc
cctgtcttcttttctagCTACTACGCCGTCCTGTATCCAATGGTGTACCCCATGAAGATCACAG
GGAACCGAGCTGTGATGGCTCTCGTCTACATCTGGCTCCACTCTCTCATTGGCTGT
CTGCCGCCCCTATTTGGTTGGTCATCGGTGGAGTTTGATGAGTTCAAGTGGATGTG
TGTGGCCGCGTGGCACCAGGAACCCGGCTACACCATTTTCTGGCAGATCTGGTGT
GCCCTGTTCCCCTTTCTCATCATGCTAGTGTGCTACGGTTTCATCTTCCGGGTGGC
CAGG**GcCgcGGCCgcAgcG**GTGCACTGTGGCACGGTGGTCACTGTGGAGGAGGA
CTCTCAGAGGAGCGGGAGGAAGAATTCTAGTACCTCCACTTCCTCCTCCGGCAGT
AGGAGGAATGCCCTTCAAGGAGTGGTCTATTCAGCTAACCAGTGCAAAGCCCTCAT
CACCATCCTGGTGGTCATTGGCGCCTTCATGGTCACCTGGGGCCCCTACATGGTT
GTCATTACCTCAGAGGCACTCTGGGGGAAGAACTGTGTCTCCCCAACCCTGGAGA
CTTGGGCCACATGGCTGTCCTTTACCAGTGCCATCTGCCACCCTCTGATCTACGGA
CTCTGGAACAAGACTGTGCGCAAGGAGCTCCTGGGCATGTGCTTTGGGGACCGT
TATTACCGGGAATCCTTTGTGCAGCGACAGAGGACCTCCAGGCTCTTCAGCATTTC
CAACAGGATCACAGgtaactaggaaaaagaccctcacacctcaggcagatgtcacccggggtccttcccagtg
gctaagggcagtgtcagggtggctgtggtctcaaggctgaagcggccgcGAAGTTCCTATTCTCTAGAAA
GTATAGGAACTTCattctaccgggtaggggaggcgcttttcccaaggcagtctggagcatgcg

B

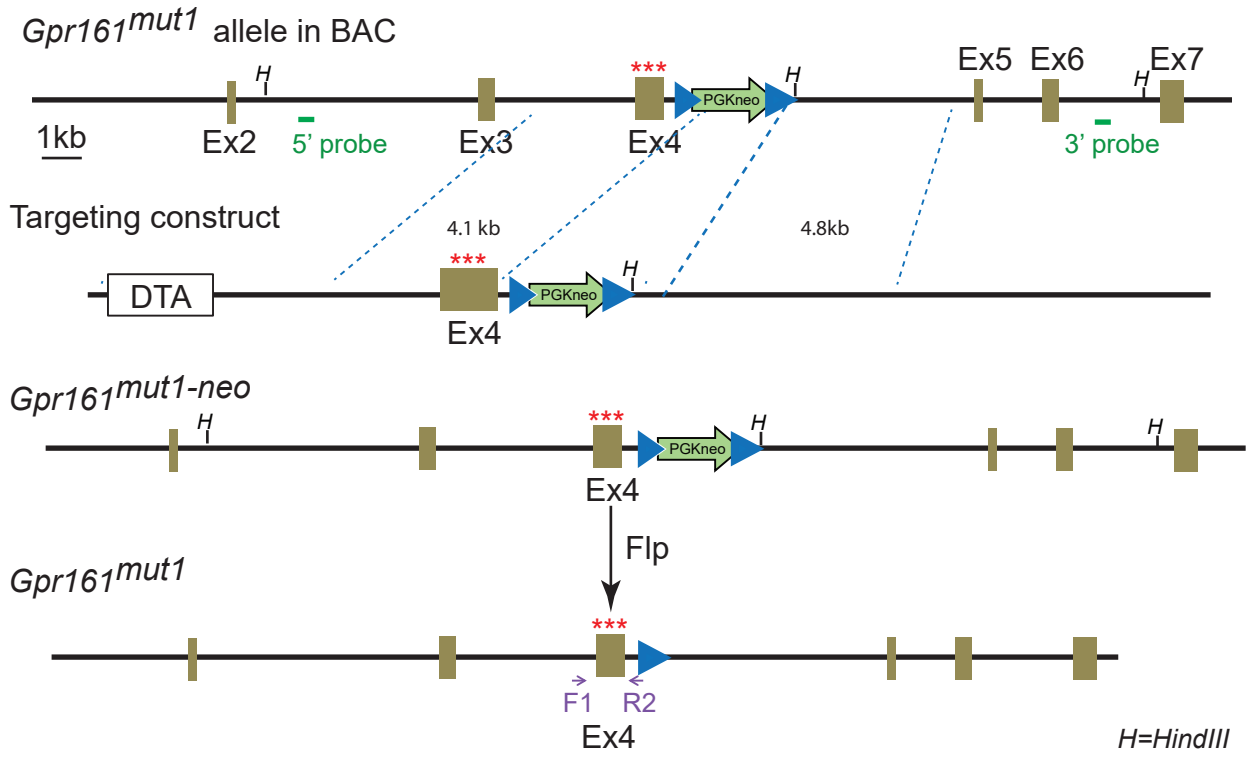

Hwang_Figure 2-Supplement 2

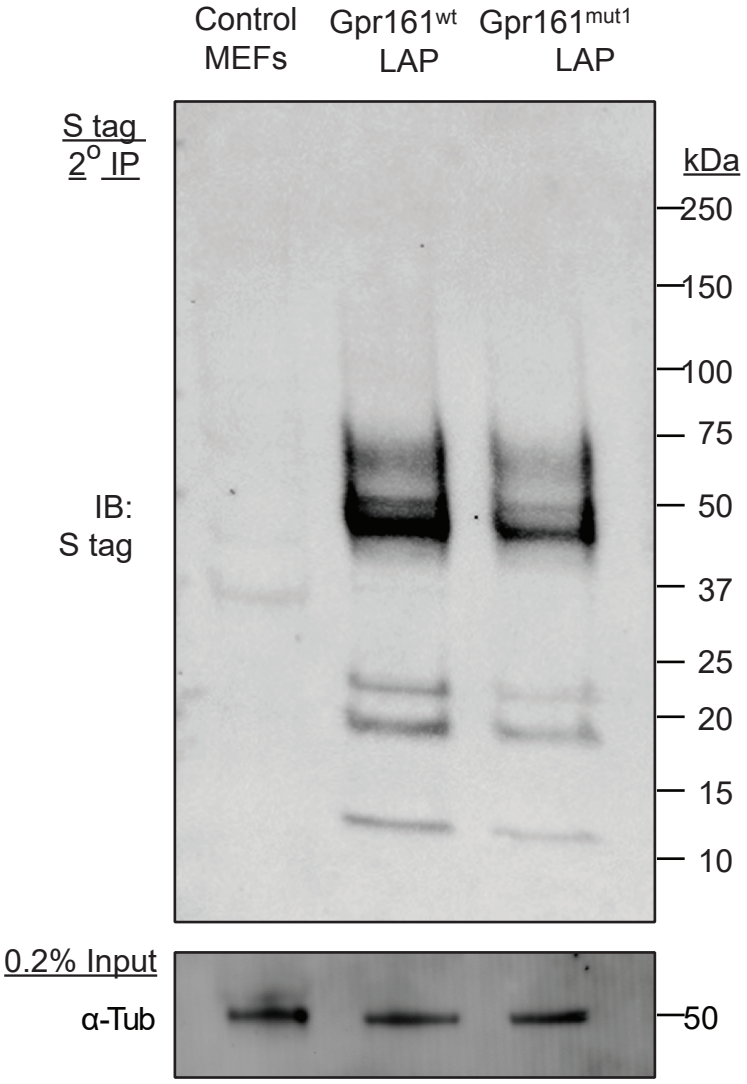

Hwang_Figure 2- Supplement 3

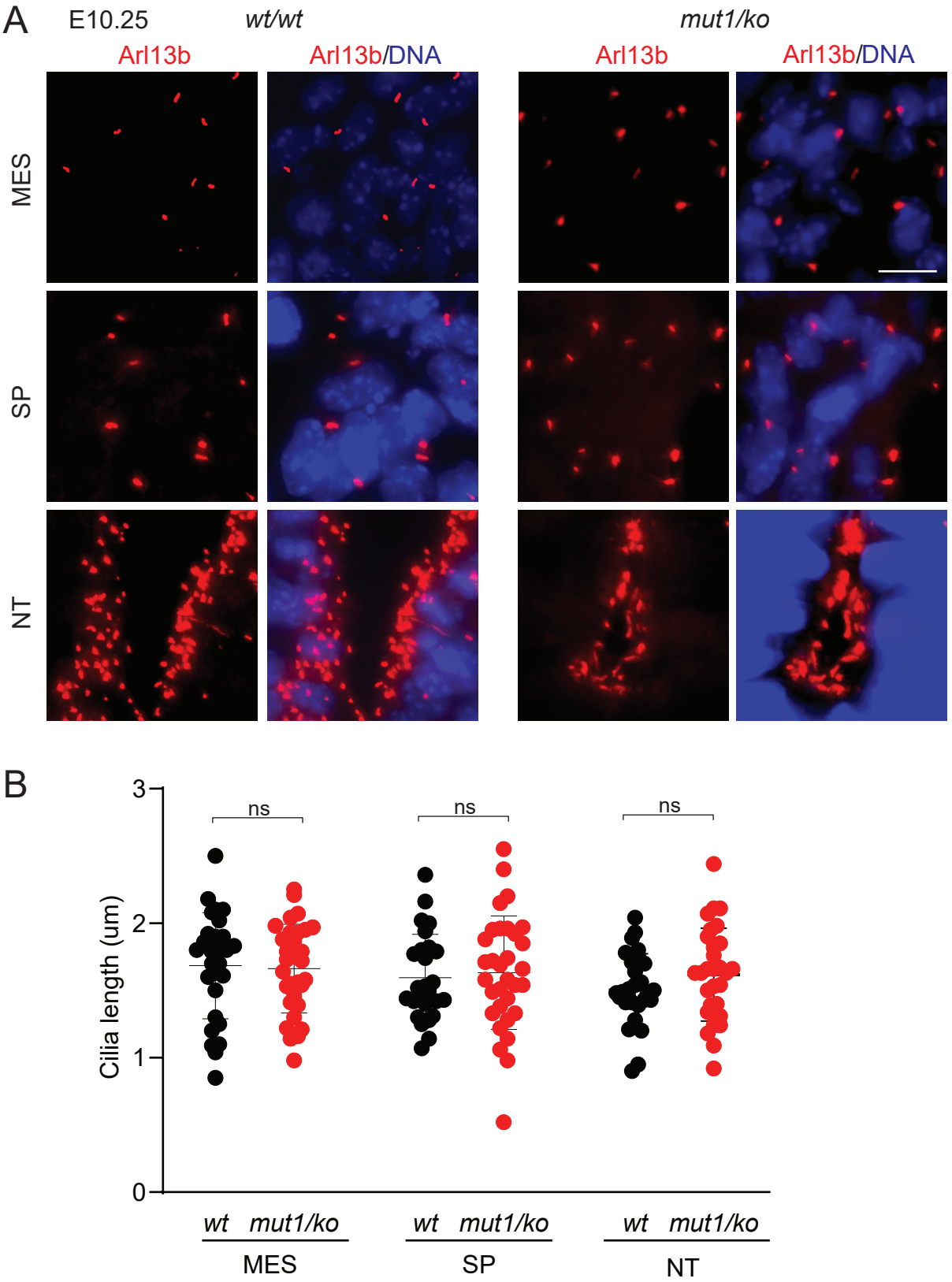

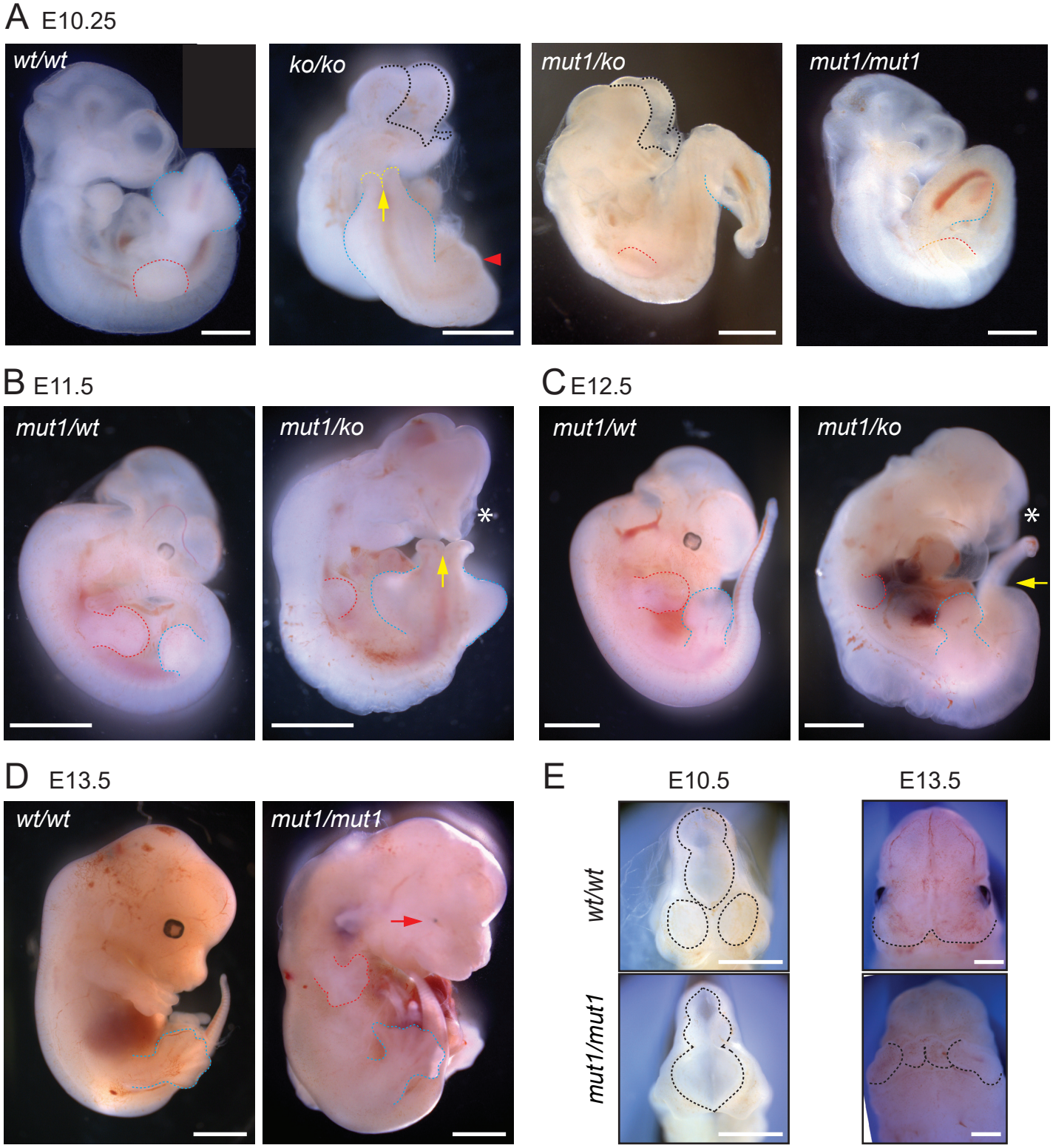
A E10.25
wt/wt
ko/ko
mut1/ko
mut1/mut1
B E11.5
mut1/wt
mut1/ko
*
C E12.5
mut1/wt
mut1/ko
*
D E13.5
wt/wt
mut1/mut1
E
E10.5
E13.5
wt/wt
mut1/mut1

Hwang_Figure 4

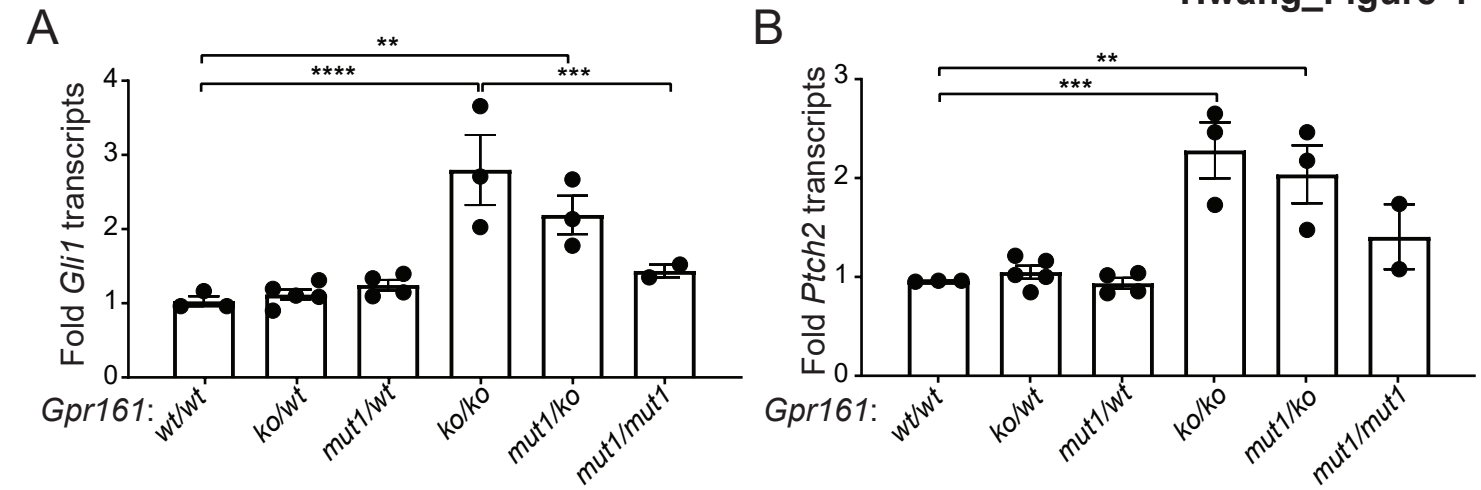

C

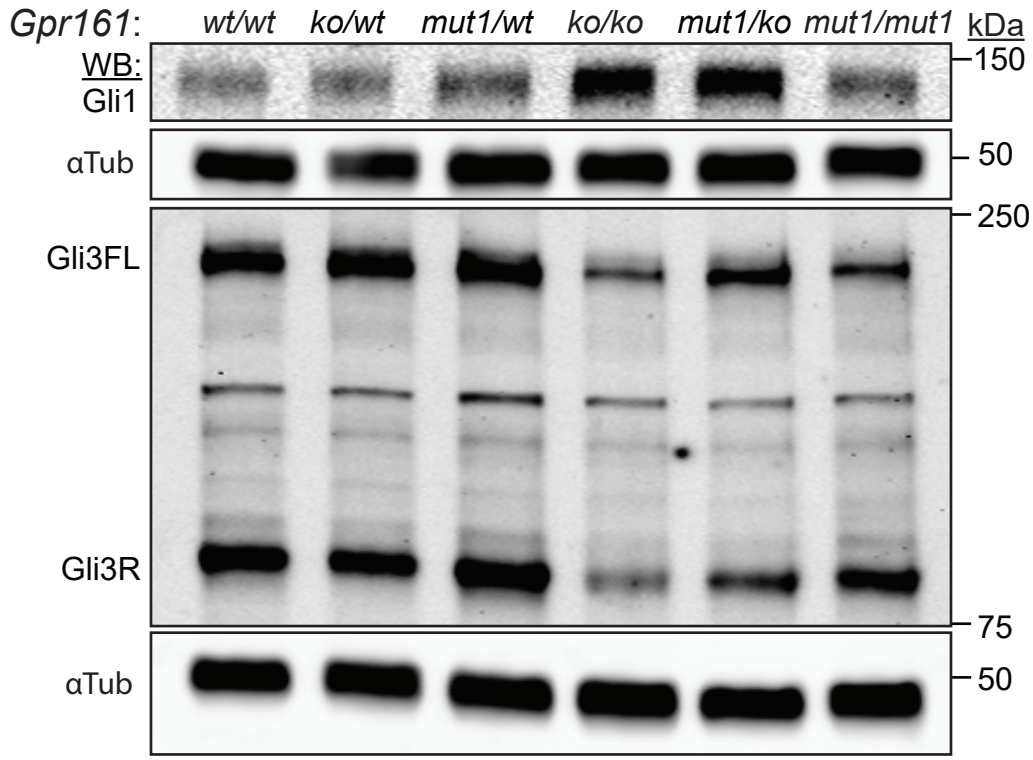

	wt/wt	ko/wt	mut1/wt	ko/ko	mut1/ko	mut1/mut1
Gli1	1.00	1.26±0.28	1.07±0.14	1.79±0.40	1.63±0.43	1.74±0.82
Gli3FL	1.00	1.00±0.14	1.01±0.05	0.45±0.17***	0.71±0.17	0.75±0.39
Gli3R	1.00	0.71±0.14	0.92±0.18	0.35±0.20***	0.47±0.16***	0.73±0.27
Gli3FL/R	0.73±0.11	1.09±0.09	0.81±0.03	1.09±0.11*	1.44±0.27***	0.67±0.01

D

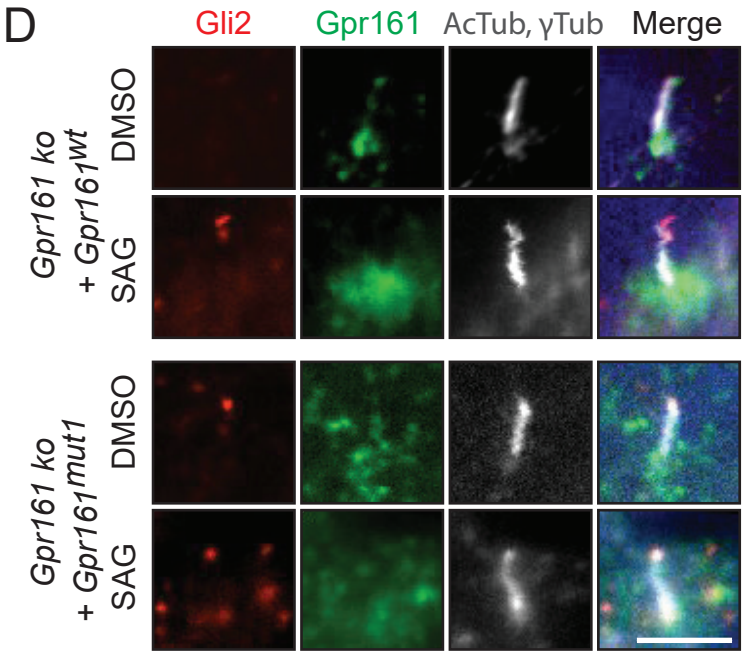

E

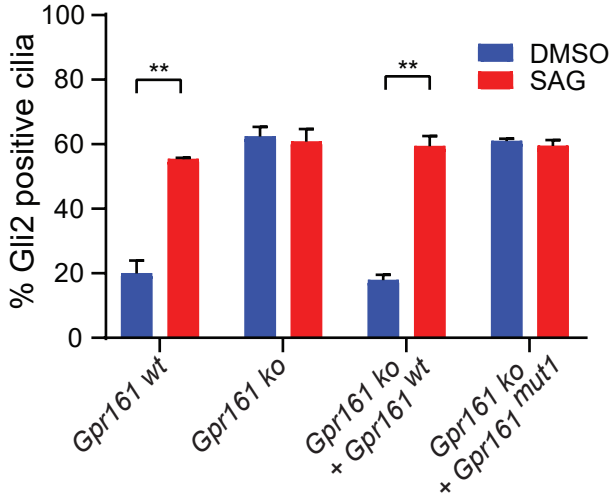

Hwang_Figure 4- Supplement 1

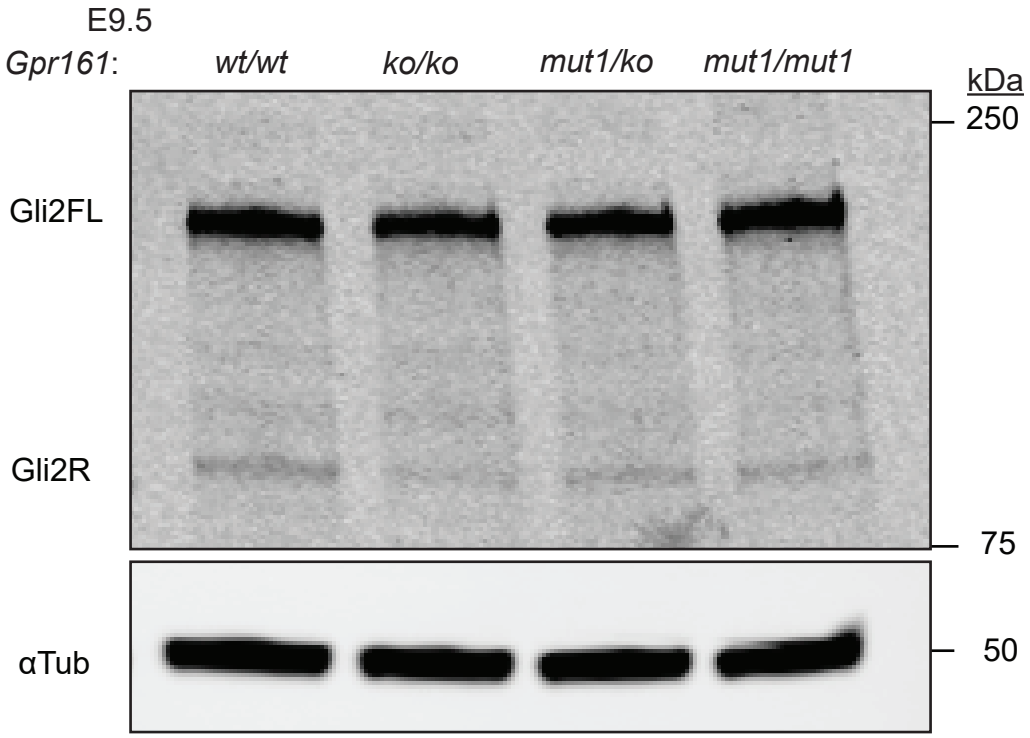

Gli2FL	1.00	1.01±0.31	1.06±0.34	1.74±1.09
Gli2R	1.00	0.76±0.03	0.80±0.14	0.92±0.06

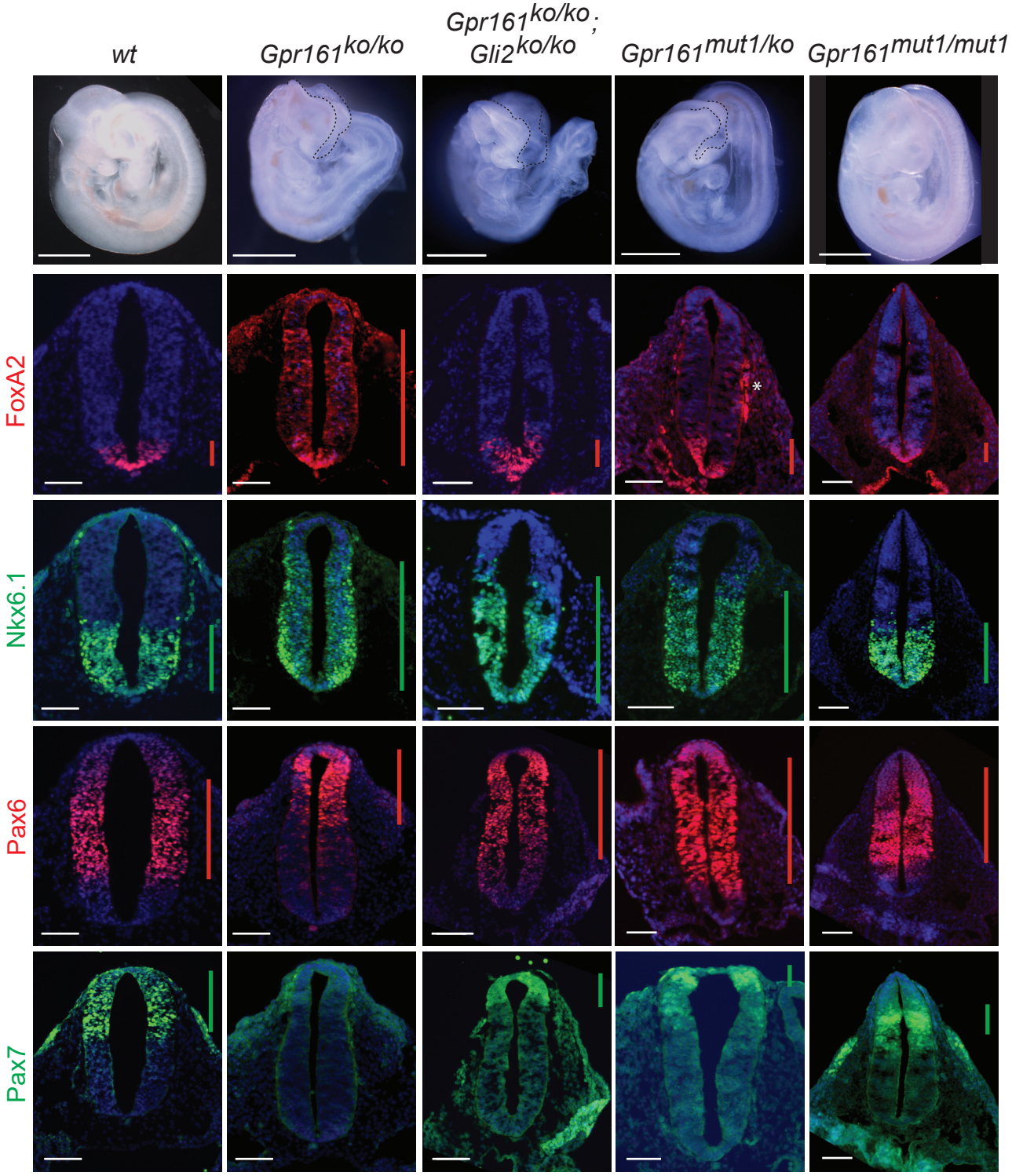
wt
Gpr161ko/ko
Gpr161ko/ko ; Gli2ko/ko
Gpr161mut1/ko
Gpr161mut1/mut1
FoxA2
Nkx6.1
Pax6
Pax7
*

Hwang_Figure 5-Supplement 1

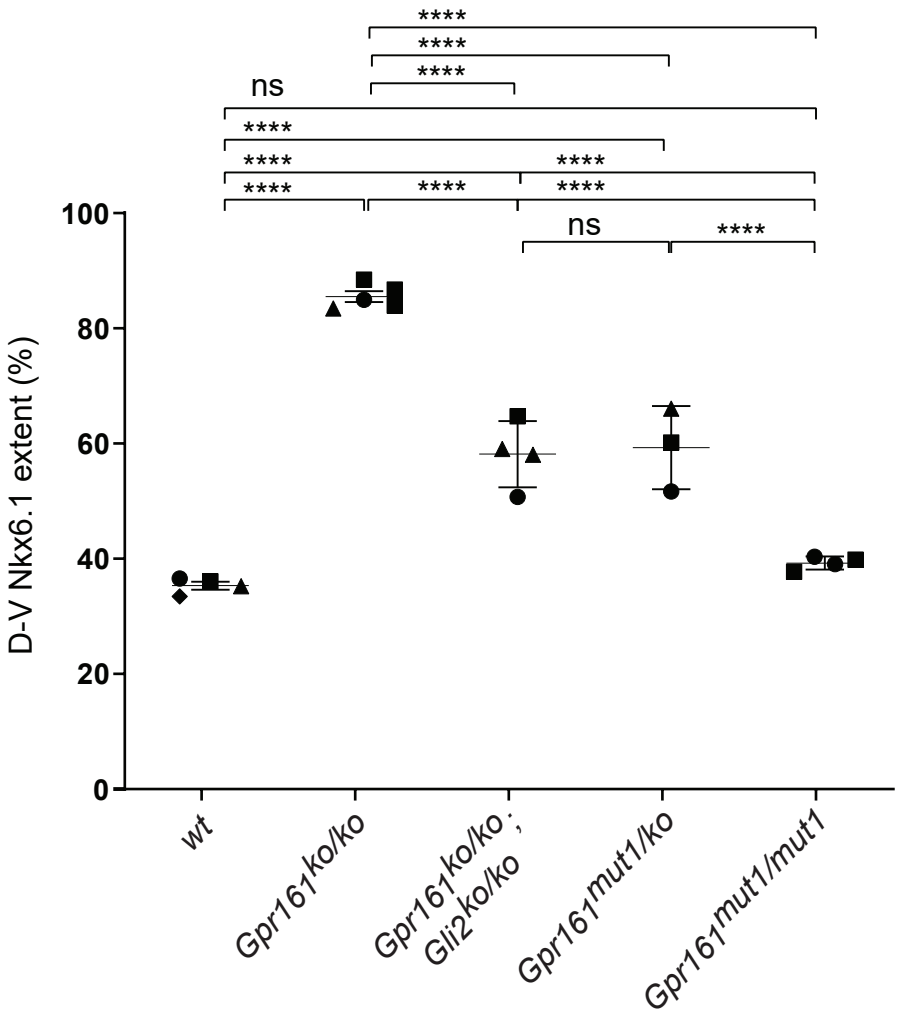

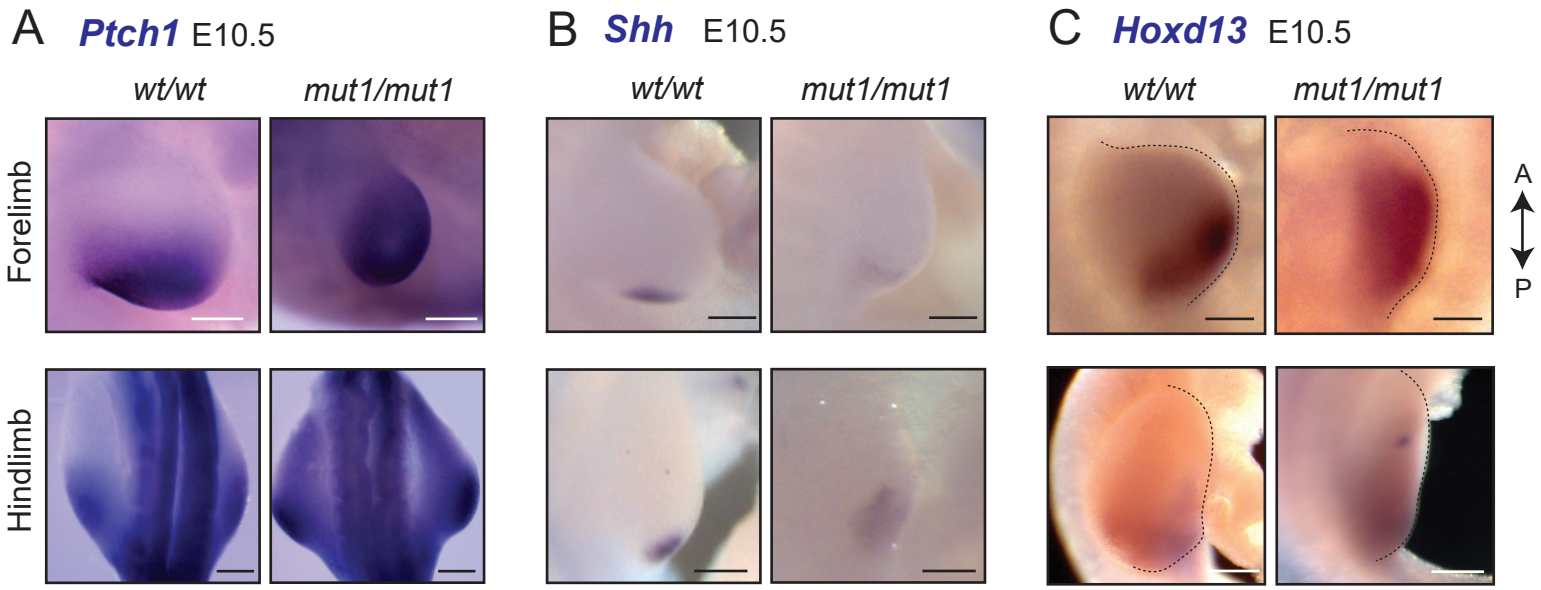

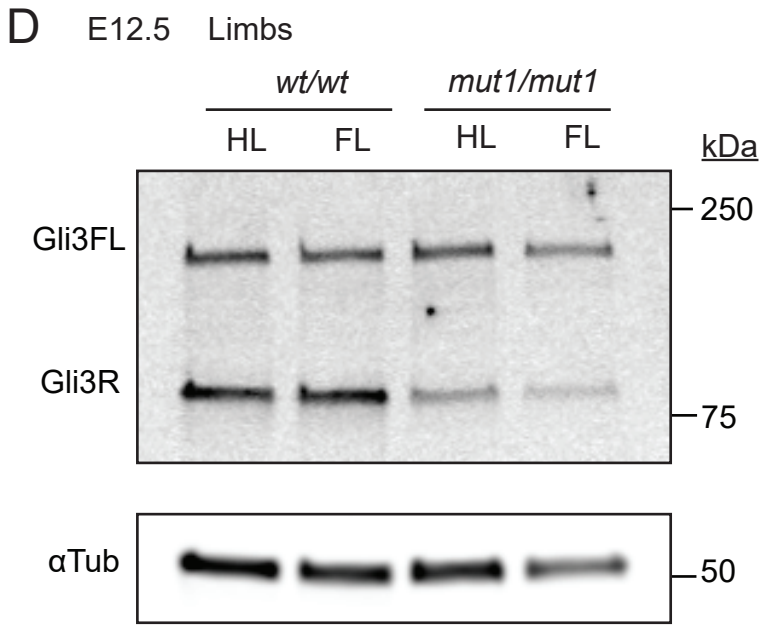

	wt/wt HL	wt/wt FL	mut1/mut1 HL	mut1/mut1 FL
Gli3FL	1.00	1.00	0.91±0.20	0.97±0.07
Gli3R	1.00	1.00	0.48±0.08**	0.39±0.13**
Gli3FL/R	0.68 ±0.13	0.55 ±0.07	1.31 ±0.41	1.74 ±0.89*

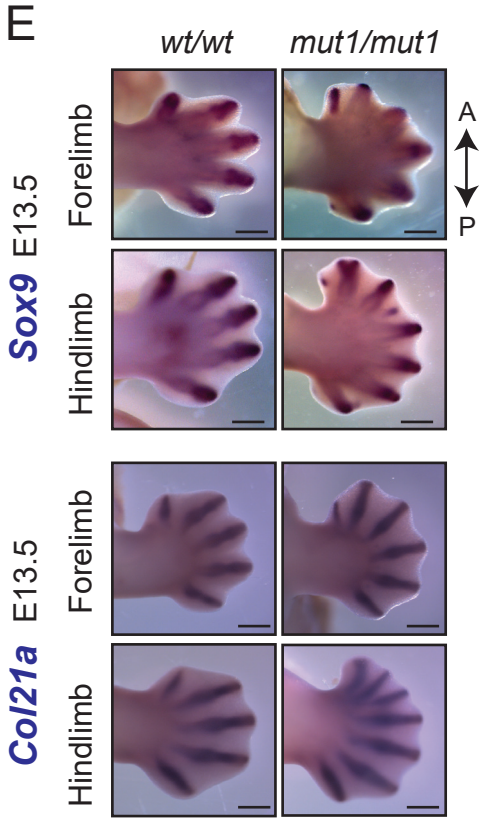

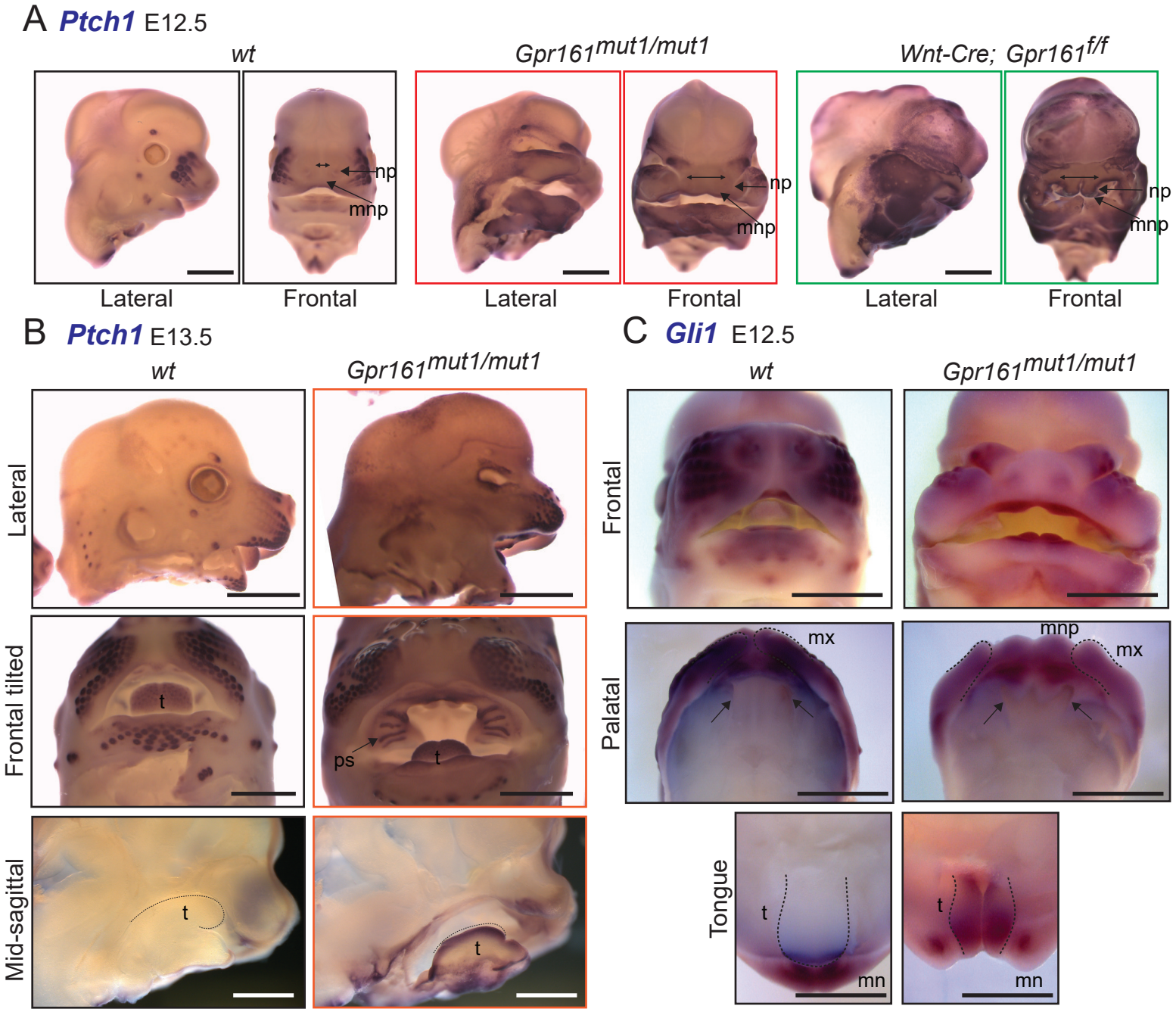
A Ptch1 E12.5
wt
Gpr161mut1/mut1
Wnt-Cre; Gpr161f/f
np
mnp
Lateral
Frontal
B Ptch1 E13.5
wt
Gpr161mut1/mut1
Lateral
Frontal tilted
Mid-sagittal
t
ps
C Gli1 E12.5
Frontal
Palatal
Tongue
mx
mnp
mn

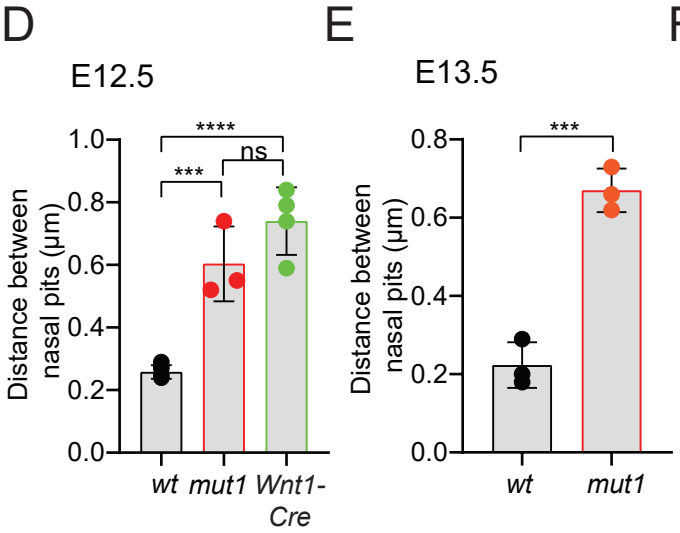
D
E12.5
E
E13.5
Distance between nasal pits (µm)
1.0
0.8
0.6
0.4
0.2
0.0
****
***
ns
wt
mut1
Wnt1-Cre

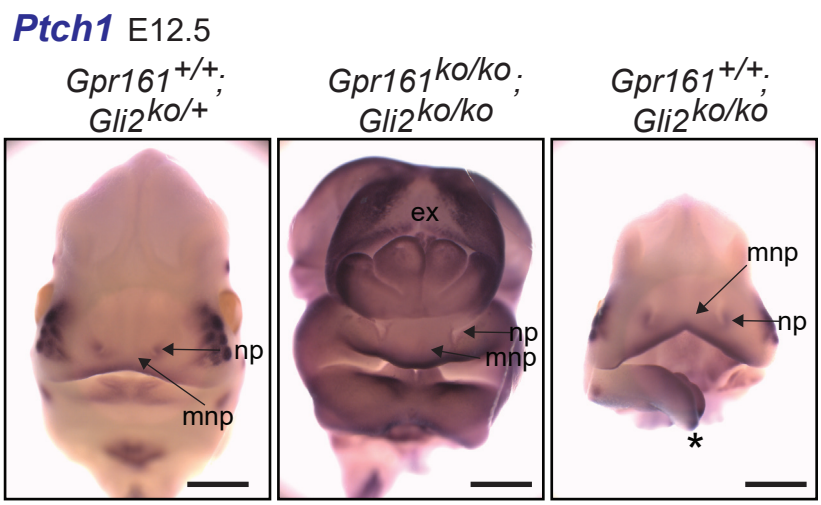
F Ptch1 E12.5
Gpr161+/+; Gli2ko/+
Gpr161ko/ko; Gli2ko/ko
Gpr161+/+; Gli2ko/ko
np
mnp
ex
*

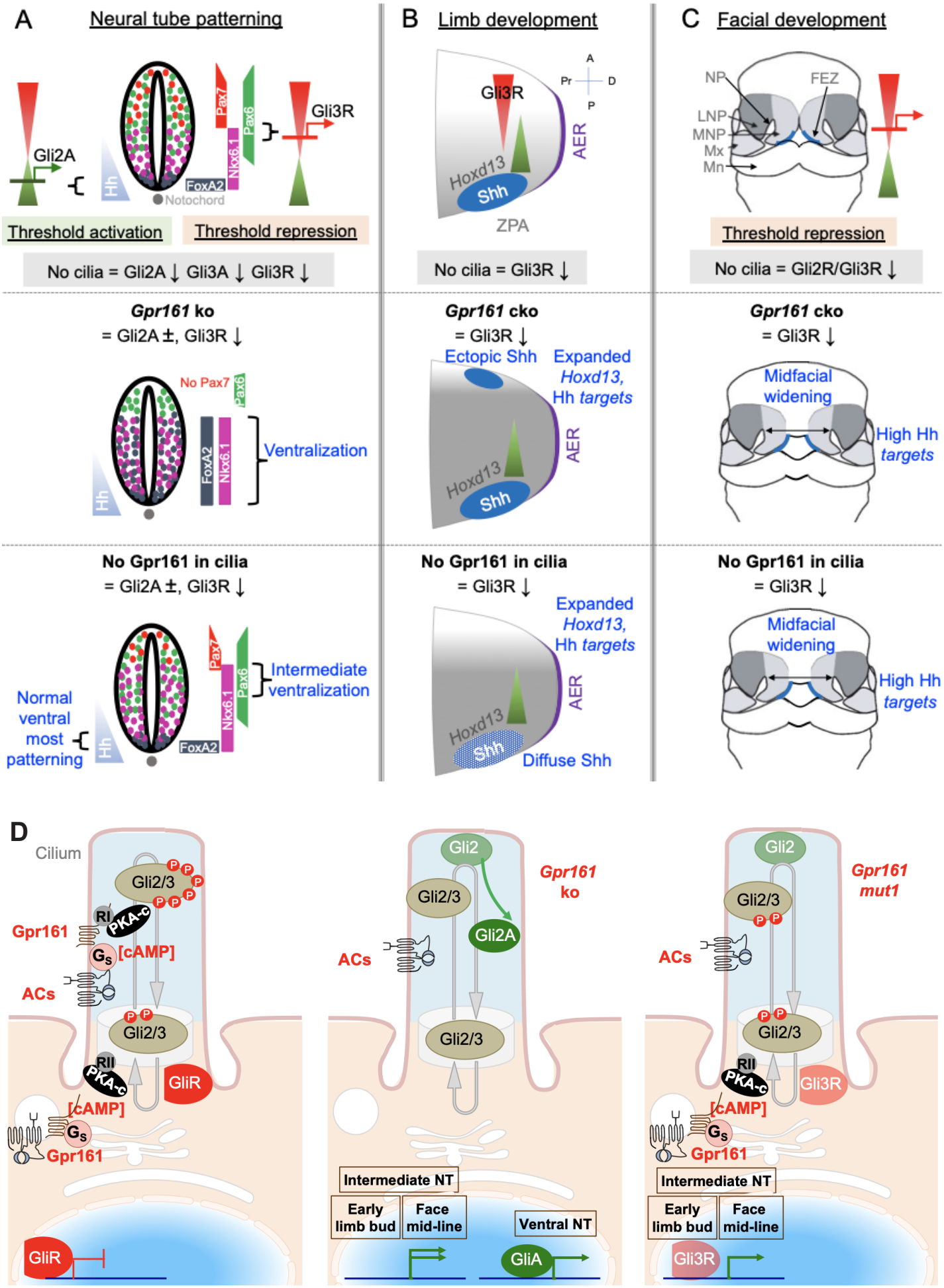
A
Neural tube patterning
Gli2A
Hh
Pax7
Pax6
Nkx6.1
FoxA2
Notochord
Gli3R
Threshold activation
Threshold repression
No cilia = Gli2A ↓ Gli3A ↓ Gli3R ↓
Gpr161 ko
= Gli2A ±, Gli3R ↓
No Pax7
Ventralization
No Gpr161 in cilia
= Gli2A ±, Gli3R ↓
Intermediate ventralization
Normal ventral most patterning
B
Limb development
Gli3R
Hoxd13
Shh
AER
ZPA
A
Pr
D
P
No cilia = Gli3R ↓
Gpr161 cko
= Gli3R ↓
Ectopic Shh
Expanded Hoxd13, Hh targets
No Gpr161 in cilia
= Gli3R ↓
Diffuse Shh
C
Facial development
NP
FEZ
LNP
MNP
Mx
Mn
Threshold repression
No cilia = Gli2R/Gli3R ↓
Gpr161 cko
= Gli3R ↓
Midfacial widening
High Hh targets
No Gpr161 in cilia
= Gli3R ↓
D
Cilium
Gli2/3
RI
PKA-c
Gpr161
Gs
[cAMP]
ACs
RII
GliR
Gli3R
Gli2
Gli2A
Gpr161 ko
Gpr161 mut1
Intermediate NT
Early limb bud
Face mid-line
Ventral NT
GliA